



Extreme variability of the tropical tropopause over the Indian monsoon region

Vanmathi Annamalai¹ · Sanjay Kumar Mehta¹

Received: 13 July 2021 / Accepted: 16 March 2022 / Published online: 30 March 2022
© The Author(s), under exclusive licence to Springer-Verlag GmbH Germany, part of Springer Nature 2022

Abstract

The extreme variability of the tropical tropopause may serve as an important factor in understanding the critical conditions of dynamical and radiative coupling between the troposphere and stratosphere. The extreme variability of the cold point tropopause (CPT) temperature (T_{CPT}) and height (H_{CPT}) are examined over a tropical station, Gadanki (13.45° N, 79.2° E), using high-resolution radiosonde data during 2006–2014. We identified the extremely cold, warm, high, and low tropopauses. The extremely cold (warm) tropopause is defined as the T_{CPT} lesser (greater) than the lower (upper) limit of the two standard deviations of its climatological monthly mean. While the extremely high (low) tropopause is defined as the H_{CPT} greater (lesser) than the upper (lower) limit of the two standard deviations of its climatological monthly mean. In total, 161 cases comprising extremely cold (52), warm (30), high (57), and low (22) are observed. The extremely cold (187.2 ± 1.60 K, 17.3 ± 0.52 km), warm (194.2 ± 1.78 K, 16.9 ± 0.89 km), high (191.7 ± 1.78 K, 18.2 ± 0.55 km), and low (191.8 ± 2.11 K, 16.2 ± 0.38 km) tropopauses occur without preference of season. However, these extreme tropopause cases occur independently and show distinct thermal structures. The thermal structures of the extremely cold tropopause cases are often sharper, whereas the extremely warm, high, and low tropopause cases are broader. Water vapor and ozone concentrations are found to be high for the extremely warm tropopause and low for the extremely cold tropopause. Under the shallow convection, extreme temperature profiles, in general, show prominent warming between 8 and 14 km while anomalous cooling (warming) just below (above) the CPT. Plausible mechanisms responsible for extreme tropopause variabilities such as deep convection, equatorial wave propagation, transports of water vapor and ozone, and potential vorticity intrusions are examined.

Keywords Tropical tropopause · Convection · Water vapour · Ozone · Temperature · PV intrusions

1 Introduction

The tropospheric temperature is maintained by convective and radiative (e.g., water vapor cooling) processes, while radiative processes (e.g., ozone heating) drive the stratospheric temperature. Thus, tropopause as the boundary between troposphere and stratosphere forms in response to achieve the radiative-convective equilibrium. Over the tropics, the simple temperature minimum (or “cold point”) in the troposphere distinctly marks the tropopause is called the cold point tropopause (CPT) (Selkirk 1993). Though

tropopause acts as a lid on the troposphere and provides a physical barrier for the stratosphere-troposphere exchange (STE) process (Holton et al. 1995), it is the gateway for most of the stratospheric water vapor. Dynamical processes such as deep convection (thunderstorms and cyclonic activities), planetary wave propagation, sudden stratospheric warmings (SSW) not only promote STE processes but also causes extreme tropopause variabilities. However, the extremeness of these processes and their effects on tropical tropopause are not known entirely yet. The tropical tropopause may be extremely cold, warm, high, and low. For example, the occurrence of the coldest tropopause may have a direct bearing on the low concentrations of stratospheric water vapor. Hence, it controls the stratospheric chemistry by protecting the ozone destruction (Fueglistaler et al. 2009).

Observations of the temperature profiles in the upper troposphere and lower stratosphere (UTLS) region reveal various thermal structures such as broader, sharper, and

✉ Sanjay Kumar Mehta
ksanjaym@gmail.com

¹ Research Institute/Atmospheric Observations and Modelling Laboratory, Department of Physics, SRM Institute of Science and Technology, Kattankulathur, Chennai, Tamil Nadu, India

multiple tropopauses. The broader tropopause mainly occurs over the subsidence region and is generally warmer (Kim and Son 2012; Schmidt et al. 2004; Seidel et al. 2001). Whereas sharper and colder tropopauses typically occurs over the regions of the active convection centers. Multiple tropopauses form due to planetary wave activities, cirrus cloud occurrence, and horizontal advection (Añel et al. 2008; Mehta et al. 2011a; Reid and Gage 1996). Tropical tropopause varies on different time scales ranging from the diurnal (hourly variations) to long-term scales. Such large temporal variations of the tropical tropopause are linked to various atmospheric processes. Non-migrating tides, convection, and planetary wave activities explain the diurnal, sub-daily, and day-to-day variations of the tropical tropopause (Jain et al. 2006; Matsuno 1966; Mehta et al. 2010; Norton 2006; Randel and Wu 2005; Reid and Gage 1996; Satheesan and Murthy 2005; Tsuda et al. 1994; Yamamoto et al. 2003). Tropospheric convection and stratospheric Brewer-Dobson circulation explain the seasonal and annual variations (Reid and Gage 1996; Son et al. 2011). While quasi-biennial oscillations (QBO), El Niño Southern Oscillation (ENSO), solar cycle, and volcanic activities are responsible for the inter-annual variabilities of the tropical tropopause (Seidel et al. 2001). Anthropogenic activities such as increased greenhouse gases are connected to long-term variabilities of the tropical tropopause (Wang et al. 2012).

Several studies on the tropical tropopause have been carried out using high-resolution radiosonde data (Jain 2011; Mehta et al. 2010; Sunilkumar et al. 2013), reanalysis data (Highwood and Hoskins 1998; Randel et al. 2000), and satellite measurements (Kim and Son 2012; Mehta et al. 2011a; Ratnam et al. 2005). These studies emphasized that convection plays a dominant role in the tropical tropopause variability. During the convection, the environmental lapse rate decreases from the surface to the mid-troposphere while increases in the cloud layer and the temperature reaches a minimum near the cloud-top height in the upper troposphere resulting in a secondary tropopause (Biondi et al. 2012; Shi et al. 2017). The secondary tropopause forms when deep convection does not reach the CPT. Note that the tropopause cools and the lower stratosphere warms when convection is nonpenetrative (Xian and Fu 2015). Generally, tropical tropopause forms at a lower altitude during deep convection events (Mehta et al. 2010; Muhsin et al. 2018). However, tropical tropopause can occur at extremely high altitudes during the overshooting convection, and moist air can even intrude into the lower stratosphere. These rare convective overshoots followed by strong downdrafts can weaken the stability of the tropical tropopause layer (TTL) region (Kumar 2006). The overshooting convection is characterized by warm anomalies in the mid-troposphere, cold anomalies at the CPT, and lower stratosphere. Such stratospheric

intrusions leave the signature of high ozone concentrations and low relative humidity.

The convective systems are also known to be important processes for the extremely cold tropopause (Jain et al. 2010). Such coldest tropopause could result from convective overshoot followed by irreversible mixing (Danielsen 1982; Kim and Dessler 2004) or diabatic cooling by convective systems (Sherwood et al. 2003). The relative locations of the deep convections and extremely cold tropopause could be important in determining the entry of the tropospheric air into the lower stratosphere (Jain et al. 2010; Kim et al. 2018; Pommereau and Held 2007). The wave activities associated with convection and strong background horizontal wind (e.g., tropical easterly jet stream) may lead to the spatial distribution of the extremely cold tropopause over substantial distances (Bhat 2003; Kuang and Bretherton 2004). For example, Jain et al. (2010) reported that the extremely cold CPT temperatures (≤ 191 K) are often observed during the monsoon season over the Bay of Bengal (BOB) and adjoining areas. Borsche et al. (2007) have reported the observational evidence that extremely cold tropical tropopauses reach about -100 °C and indicated the need for examining the meteorological condition behind such extreme cold tropical tropopauses.

The tropical convection can also be triggered due to potential vorticity (PV) intrusion associated with SSW events (Dixon et al. 2012; Kodera 2006; Resmi et al. 2013). Such PV intrusions can bring ozone-rich stratospheric air into the upper troposphere (Waugh and Polvani 2000). Over Gadanki, Nath et al. (2013) observed a strong PV intrusion during the SSW event during 2009. The tropical tropopause cooling was observed in association with convection following the SSW event 2009 (Yoshida and Yamazaki 2011). Resmi et al. (2013) examined several major SSW events and found that cooling becomes intense with the peak phase of SSW. Recently, Roy et al. (2021) examined the intrusion of the ozone-rich air during El-Niño over the Indian region and found an anomalous cooling due to the transport of extratropical cold air that offset the heating due to enhanced ozone. Thus, the coupling between tropical convection and stratospheric events might profoundly impact the extreme variation of the CPT.

Mehta et al. (2010) reported that the correlation between CPT temperature and height degrades from seasonal to day-to-day scales due to dominance of the short time scales processes such as cold or hot air advection, stratospheric air entrainment, and cirrus clouds formation. Sunilkumar et al. (2013) also observed a poor negative correlation or positive correlation between the monthly mean CPT temperature and height, mainly over the off-equatorial region where the surface or tropospheric process (Shepherd 2002) is very strong, especially during the Asian summer monsoon season. They suggested the combined effects of the dynamics and

radiation are responsible for such a poor negative correlation between CPT height and temperature. Thus, the knowledge of the extreme variability in the tropical tropopause will be useful to understand the STE processes and associated radiative balance of the UTLS as well as global circulation (Fueglistaler and Haynes 2005; Gettelman, 2010).

On a day-to-day scale, CPT height and temperature sometimes vary extremely. However, it has been ignored partly due to its rare occurrence and partly due to complex UTLS processes. The complexity arises due to interlinked physical, chemical, and dynamical processes. In this paper, we have attempted to examine the extreme variation of the CPT using regular radiosonde data at 17:00 IST over Gadanki (13.5°N, 79.2°E) during 2006–2014. The objectives of the present study are to (1) define the extreme tropopause cases occurring during different seasons, (2) examine the thermal structures of the extreme tropopauses, and (3) explore the plausible roles of the convection, PV intrusion, radiative heating due to water vapor and ozone, and equatorial wave propagation in the occurrence of the extremely cold, warm, high and low tropopause cases. Section 2 describes the data and methodology, and results are presented in Sect. 3, followed by discussions in Sect. 4. Results are summarized in Sect. 5.

2 Data and methodology

2.1 GPS Radiosonde data

We have used high-resolution GPS radiosonde (Väisälä RS-80, Väisälä RS-92, and Meisei RD-06G) temperature data regularly observed almost every day at ~17:00 IST (Indian Standard Time (IST) = Universal Time (UT) + 05:30 h) during 18 April 2006–November 2014 over Gadanki (13.5°N, 79.2°E), a tropical station, located at 375 m above mean sea level. The uncertainties in temperature retrieved from different receivers are less than 0.5 K (Kizu 2018; Vömel et al. 2007). The temperature profiles are collected with an altitude resolution of 25–30 m (sampled at 5 s intervals) from RS-80 (April 2006 to March 2007) and 10 m (sampled at 2 s intervals) from RS-92 (17 July 2006 to 31 August 2006) and Meisei (May 2007 to November 2014) radiosondes. The entire data with different altitude resolutions (10 m and 25–30 m) is uniformly gridded to 100 m altitude resolution. Quality checks are then applied to remove any outliers or very high-frequency fluctuations arising due to various reasons such as random motions of the balloons to ensure high quality in the data (Mehta et al. 2011a). In total, 2487 radiosonde soundings are available with major data gaps during December 2006, April–May 2007, March 2011, December 2012, January–February 2013, and April 2013 due to some technical reasons. Out of which, 42 are rejected

either due to balloon burst height below the tropopause or due to bad data quality. The remaining 2445 profiles of temperature are utilized to obtain the minimum temperature and corresponding altitude which are represented as the CPT temperature (T_{CPT}) and height (H_{CPT}).

2.2 Infrared brightness temperature (IRBT) data

To investigate the role of deep convection on the extreme variability of the tropopause, we have used globally merged IRBT data obtained from the national weather service Climate Prediction Centre, NOAA. IRBT data is a globally merged, full-resolution (up to ~4 km) IR data formed from the ~11 μm IR channels aboard the GMS-5, GOES-8, Goes-10, Meteosat-7, and Meteosat-5 geostationary satellites. The IRBT data is available with a time resolution of one hour and spatial resolution of $0.03^\circ \times 0.03^\circ$ latitude–longitude. In this study, we have averaged the IRBT data into $0.5^\circ \times 0.5^\circ$ (latitude–longitude) centered to Gadanki and within ± 1.5 h of 17:00 IST. The convective cloud top height (H_{CCT}) for each extreme tropopause case is obtained from the corresponding radiosonde temperature profiles as the altitude equivalent to averaged IRBT.

2.3 Microwave limb sounder (MLS) data

MLS of the Earth Observing System (EOS) on-board NASA's EOS Aura satellite is operational since August 2004. Aura-MLS provides high-resolution data from the ground to about 90 km.

MLS crosses Gadanki, nearly ~13.35 N and ~77–80 E at the local solar time 01:40 am/pm on every 16-day cycle. We collected the MLS water vapor (H_2O) and ozone (O_3) profiles data on the days of extreme tropopause cases over the period 2006–2014. Note that radiosonde data is available at Gadanki at ~17:30 IST while MLS data at ~13:40 IST and 01:30 IST on the matching date. Water vapor profiles were retrieved from the radiance measurements of ~190 GHz rotational line and are available from the pressure levels 316 hPa to 0.02 hPa. The ozone profiles were retrieved from the radiance measurements of ~240 GHz and are available from the pressure levels 261 hPa to 0.02 hPa. In this study, water vapor and ozone profiles between the pressure levels 150 hPa and 60 hPa (~13.5–20.0 km) is obtained on the days of extreme tropopause events. The MLS water vapor and ozone pressure levels are converted to height levels using the Barometric equation.

2.4 ERA5 data

To examine the role of the Rossby wave breaking, we employed the potential vorticity (PV) data from the fifth generation of atmospheric reanalysis of European Centre

for Medium Range Weather Forecast (ECMWF) (ERA5; Hersbach et al. 2020) available at 37 pressure levels and the spatial resolution of $0.25^\circ \times 0.25^\circ$. The PV data is collected at 12 UTC (17:30 IST) within ± 0.25 -degree latitude-longitude around Gadanki for the period 2006–2014. The pressure levels are converted to height levels using the Barometric equation.

3 Results

3.1 Identification of the extreme tropopause variability

Figure 1a shows the daily radiosonde observations and their maximum altitude coverage. Almost 99% of the sonde bursts above the tropopause altitude (~ 15 – 20 km on day-to-day scales), and 90% have crossed the altitude 20 km out of the total launchings (excluding the data gaps) over Gadanki during 2006–2014 as mentioned earlier. These sondes are utilized to study the day-to-day variations of the T_{CPT} (Fig. 1b) and H_{CPT} (Fig. 1c) over 2006–2014. The 30-point running means of the T_{CPT} and H_{CPT} are also shown. Both T_{CPT} and H_{CPT} clearly show annual cycles with colder and higher CPT during the northern hemisphere (NH) winter (DJF) season and warmer and lower CPT during the NH summer (JJA) season. However, the annual cycle in H_{CPT} is better characterized when compared to T_{CPT} ; hence, their relationship

is not exactly a linear one (Mehta et al. 2011b; Reid and Gage 1996). The H_{CPT} and T_{CPT} are weakly anti-correlated (-0.30) significant at a 95% confidence level. The correlation (-0.45) slightly improves by removing or smoothing high-frequency variabilities. It indicates that these high-frequency variabilities occur without preference of the season. It is observed that T_{CPT} and H_{CPT} , though they characterize the same tropopause, may get affected differently by different atmospheric processes especially on the day-to-day scale. For example, very deep convection may push the tropopause and it may become higher and colder. However, subsidence following convection may lead to ozone transport which can radiatively warm the tropopause without changing its height.

We obtained the climatological monthly mean, 1σ (standard deviation), 2σ and 3σ variations of the T_{CPT} and H_{CPT} for 2006–2014, as shown in Fig. 2. On a day-to-day basis, CPT over Gadanki varies extremely. H_{CPT} is found to be as low as ~ 15.5 km and as high as ~ 19.5 km, whereas T_{CPT} is as cold as ~ 183 K and as warm as ~ 196 K several times. However, most of the studies present the climatology of the CPT as mean and $\pm 1\sigma$ (Mehta et al. 2010; Seidel et al. 2001), which generally does not represent these extreme variations. We have obtained the probability distributions of the T_{CPT} , H_{CPT} , ΔT_{CPT} and ΔH_{CPT} where Δ represents the day-to-day forward difference (tendency) as shown in Fig. 3. It is interesting to note that these distributions are nearly Gaussian type. It is to be noted that, over the subtropics, the distribution of the tropopause height and temperature is bimodal

Fig. 1 Timeseries of the daily a radiosonde observations and its maximum height coverage, variation of the b T_{CPT} and c H_{CPT} observed over Gadanki during 2006–2014. The heavy solid curves in the lower panels (b, c) represent the 30-point running mean

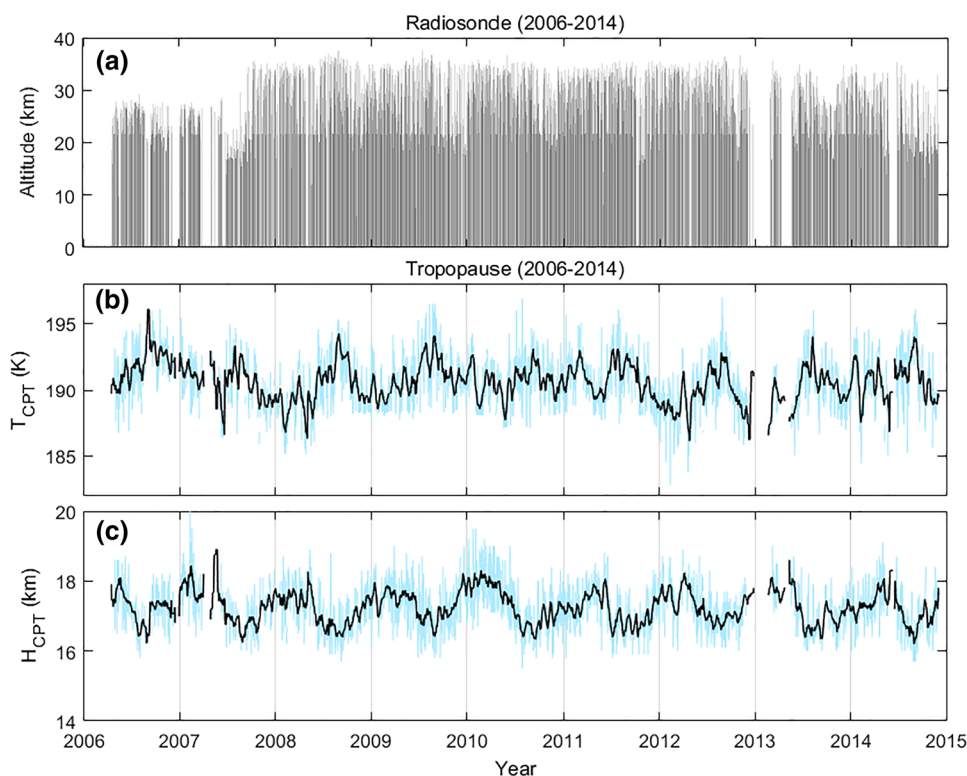


Fig. 2 The day-to-day variations of the **a** T_{CPT} and **b** H_{CPT} from January to December overplotted for each year between 2006 and 2014. Their climatological monthly means (μ) and one, two and three standard deviations (σ) over the period 2006–2014 are superimposed on them

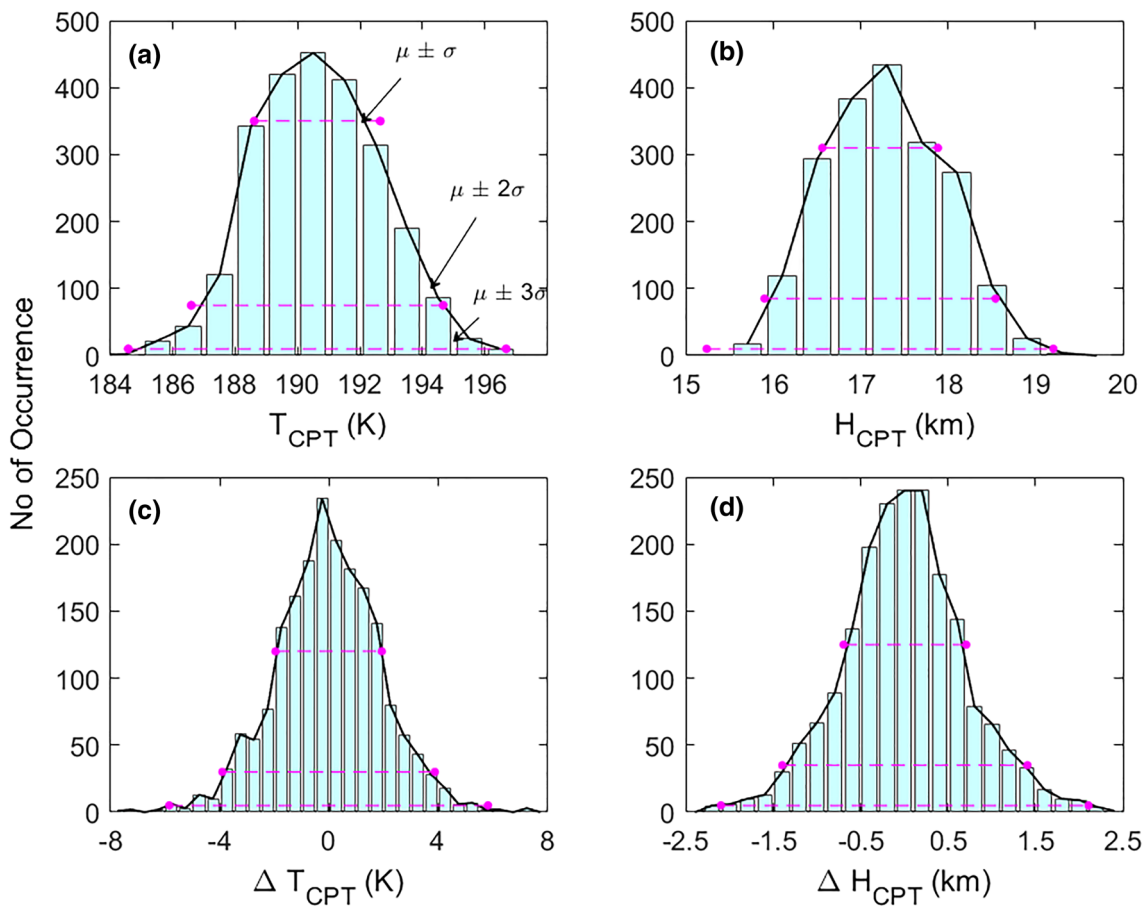
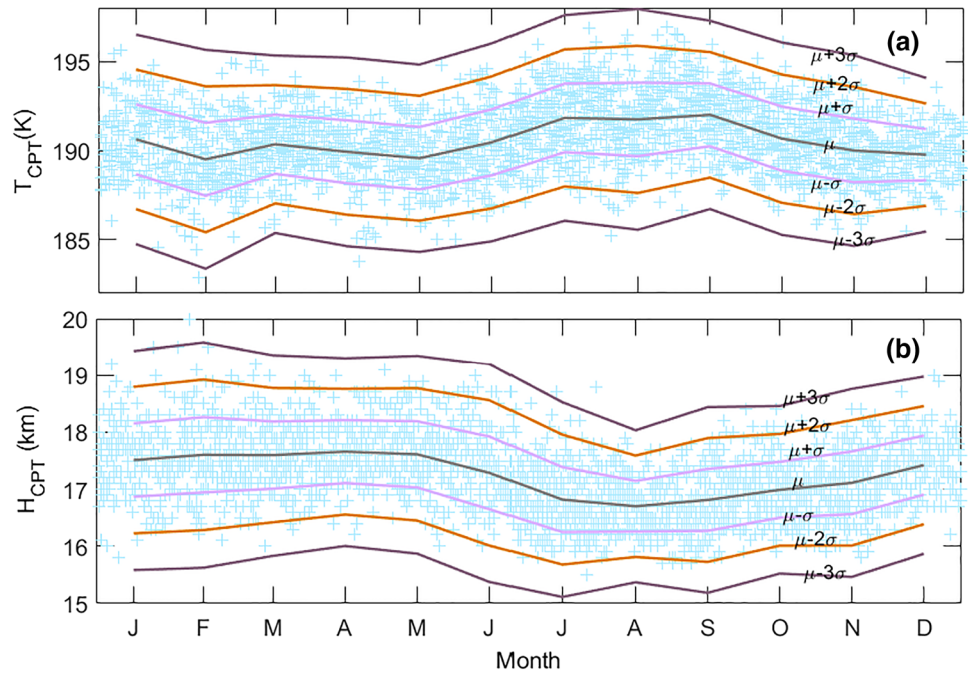


Fig. 3 Probability distribution of the day-to-day values of the **a** T_{CPT} , **b** H_{CPT} , **c** ΔT_{CPT} and **d** ΔH_{CPT} along with $\mu \pm \sigma$, $\mu \pm 2\sigma$ and $\mu \pm 3\sigma$ lines indicated as horizontal dashed lines observed over Gadanki dur-

ing 2006–2014. ΔT_{CPT} and ΔH_{CPT} represent their day-to-day difference where Δ represent the forward difference

(peaks at ~12 km and ~16 km) due to the frequent occurrence of the multiple tropopause associated with the subtropical jet (STJ) (Pan et al. 2004). Whereas over Gadanki, the normal distributions of the T_{CPT} and H_{CPT} suggest that sharper tropopause occurs more frequently than the multiple and broader tropopause.

As mentioned earlier, we have 2445 observations of the T_{CPT} and H_{CPT} over 2006–2014. Out of which about 67%, 95% and 99.7% of the data fall within $\pm 1\sigma$, $\pm 2\sigma$, and $\pm 3\sigma$ respectively. There is a clear peak (mode) in the T_{CPT} (190.5 K) and H_{CPT} (17.3 km), which closely coincides with their mean T_{CPT} and H_{CPT} , respectively (see supplementary Table S1). Thus, 67% of the T_{CPT} and H_{CPT} ranges from 188.6 K to 192.6 K and 16.6 km to 17.9 km, respectively. About 28% of the T_{CPT} ranges ~185.4–190.2 K and ~191.6–195.9 K, while H_{CPT} ranges ~15.7–17.1 km and ~17.1–18.9 km. The remaining 5% varies extremely with $T_{\text{CPT}} < 188.5$ K, $T_{\text{CPT}} > 195.9$ K, $H_{\text{CPT}} < 16.5$ km, and $H_{\text{CPT}} > 17.6$ km. We termed them as the extremely cold, warm, low, and high tropopause, respectively. Over Gadanki, the distribution of the ΔT_{CPT} reveals that T_{CPT} fluctuates within ± 2 K for ~67% cases, between ± 2 K and ± 4 K for ~28% cases and greater (less) than 4 K (-4 K) for ~5% cases on a day-to-day basis (Fig. 3c). Similarly, the distribution of ΔH_{CPT} reveals that H_{CPT} fluctuates within $\sim \pm 0.7$ km for ~67% cases, between ± 0.7 km and ± 1.4 km for ~28% cases and greater (less) than 1.4 km (-1.4 km) for ~5% cases on a day to basis (Fig. 3d). Thus, when H_{CPT} (T_{CPT}) increases or decreases by 1.4 km (4 K), those cases are regarded as extreme cases. In other words, those T_{CPT} and H_{CPT} which vary more than the values 2σ from their climatological monthly mean are termed as extreme cases. The extreme variability in the T_{CPT} and H_{CPT} are identified based on the 2σ departure from their climatological monthly mean. Climatological monthly mean T_{CPT} and H_{CPT} are represented as μT_{CPT} and μH_{CPT} , respectively and their standard deviations as σT_{CPT} and σH_{CPT} , respectively. Thus, extremely cold (warm) tropopause, defined as T_{CPT} is lesser (greater) than its climatological monthly mean minus (plus) two standard deviations i.e., $\mu T_{\text{CPT}} - 2\sigma T_{\text{CPT}}$ ($\mu T_{\text{CPT}} + 2\sigma T_{\text{CPT}}$). Similarly, the extremely low (high) tropopause defined as H_{CPT} is lesser (greater) than its climatological monthly mean minus (plus) two standard deviations i.e., $\mu H_{\text{CPT}} - 2\sigma H_{\text{CPT}}$ ($\mu H_{\text{CPT}} + 2\sigma H_{\text{CPT}}$).

3.2 Temporal distributions and occurrence of the extreme tropopause

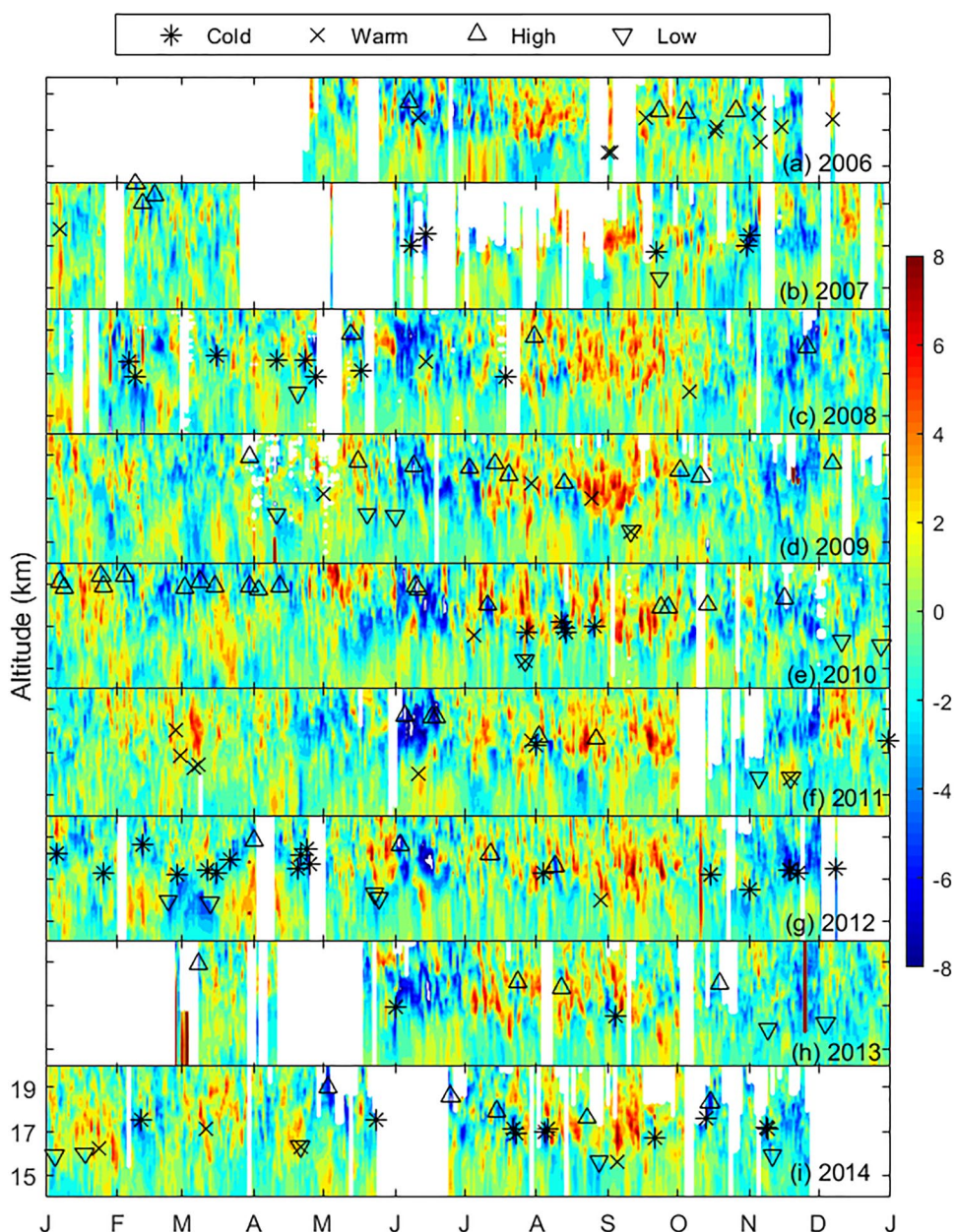
In total, 161 extreme cases of the CPT are found over the period 2006–2014, which are utilized for further analysis. Out of which 52, 30, 57, and 22 cases are found as the extremely cold, warm, high, and low tropopause, respectively. To understand the behavior of the temperature

structure neighborhood to the extreme tropopause, we have juxtaposed them over the time-height section of the temperature anomalies between altitudes 14–20 km for 2006–2014, as shown in Fig. 4. For clarity, we have also plotted the temporal distribution of the extreme H_{CPT} and T_{CPT} separately, as shown in Supplementary Fig. S1 and S2, respectively. It is clear that the extremely cold and high tropopause are distributed throughout the season and not preferably in the NH winter season. Similarly, the extremely warm and low tropopause occur randomly in all seasons, not preferably in the NH summer season. It is also evident that the extremely cold and high tropopause arise independently. That is, the extremely cold tropopause is not the extremely high one and vice versa. Similarly, the extremely warm and low tropopause also occur independently except for 4 cases.

The number of occurrences of the extremely cold, warm, high and low tropopause, their mean and standard deviation during different seasons is shown in Fig. 5. Overall, the occurrence of extreme cases is minimum during winter and maximum during the NH summer season. It indicates that the extreme cases occur throughout the year and without any preference to season. Interestingly, the extremely cold tropopause occurs more frequently during the NH summer season than in the NH winter season. It supports the earlier finding that the extremely cold tropopause occurs more frequently during the NH spring (MAM) and summer season over the Indian monsoon region (Jain et al. 2006; Newell and Gould-Stewart 1981). The extremely low tropopause occurs more frequently during the NH winter season when compared to the NH summer season. Though tropopause is higher and colder during NH winter, the extremely high tropopause frequently occurs during NH summer. During the summer monsoon season, deep convection frequently occurs over this location which could be a possible reason for the frequent occurrence of the extremely high tropopause during this season. However, as the tropopause is lower and warmer during the summer season, the extremely warm tropopause also occurs more frequently.

The seasonal mean T_{CPT} of the extremely cold cases (Fig. 5b) varies from 185.1 \pm 1.1 K (in DJF) to 187.1 \pm 0.7 K (in JJA) and their corresponding H_{CPT} (Fig. 5c) varies from 17.0 \pm 0.25 km (in JJA) to 17.5 \pm 0.53 km (in DJF). The T_{CPT} for the extremely cold cases shows a similar seasonal structure as the climatological mean T_{CPT} (190–192 K). However, T_{CPT} of the extremely cold cases are always colder by about 4–5 K from the climatological mean T_{CPT} throughout the season. The H_{CPT} for the extremely cold cases also show a similar seasonal structure as the overall monthly mean (16.8–17.5 km). However, H_{CPT} of the extremely cold cases occur at the same altitude as the climatological mean H_{CPT} . Thus, it indicates that the extremely cold tropopause needs not necessarily represent the extremely high tropopause (Fig. 5).

Fig. 4 a–i Time height sections of the temperature perturbation between 14 and 20 km embedded with the H_{CPT} for extremely cold, warm, high, and low tropopause cases over the period 2006–2014, respectively



The scatter plot between the extremely cold T_{CPT} and their corresponding H_{CPT} (Fig. 6a) shows that only three extremely cold tropopauses occur above 18 km. Out of them, the coldest tropopause ($T_{CPT} = 182.8$ K, $H_{CPT} = 18.6$ km) is occurred on 11 February 2012 (Supplementary Fig. S3a). The majority of the extremely cold tropopauses are ranging between 16.5 km to 17.5 km. It can be seen that the extremely cold tropopause even occurs as low as ~ 16.5 km with $T_{CPT} < 188$ K. The T_{CPT} for the extremely cold cases are always colder than 191 K suggesting entry of drier air into the stratosphere over Gandaki. Note that for about half of the total observations, T_{CPT} remains colder than ~ 191 K (Fig. 3) which indicates that the entry of water vapor into the stratosphere with a mixing ratio less than 3.0 ppmv. The T_{CPT}

and corresponding H_{CPT} for the extremely cold cases are moderately anti-correlated ($r = -0.53$), significant at a 95% confidence level (Fig. 6a). Note that if top three extremely cold cases (shown encircled) are excluded, T_{CPT} and H_{CPT} for the remaining 49 cases are insignificantly anti-correlated (-0.33).

Similarly, the seasonal mean T_{CPT} (Fig. 5b) for the extremely warm cases vary from 194.4 ± 0.54 K (in MAM) to 196.1 ± 0.9 K (in JJA), and their corresponding H_{CPT} (Fig. 5c) varies between 16.7 ± 0.45 km (in MAM) and 17.3 ± 0.76 km (in DJF). The T_{CPT} for the extremely warm cases are warmer by 4–5 K from the climatological mean T_{CPT} . The scatter plot between T_{CPT} and their corresponding H_{CPT} (Fig. 6b) shows that the extremely warm tropopauses

Fig. 5 Season-wise **a** occurrence of CPT **b** mean and standard deviation of the T_{CPT} and **c** mean and standard deviation of the H_{CPT} for the extremely cold, warm, high, and low cases observed during 2006–2014

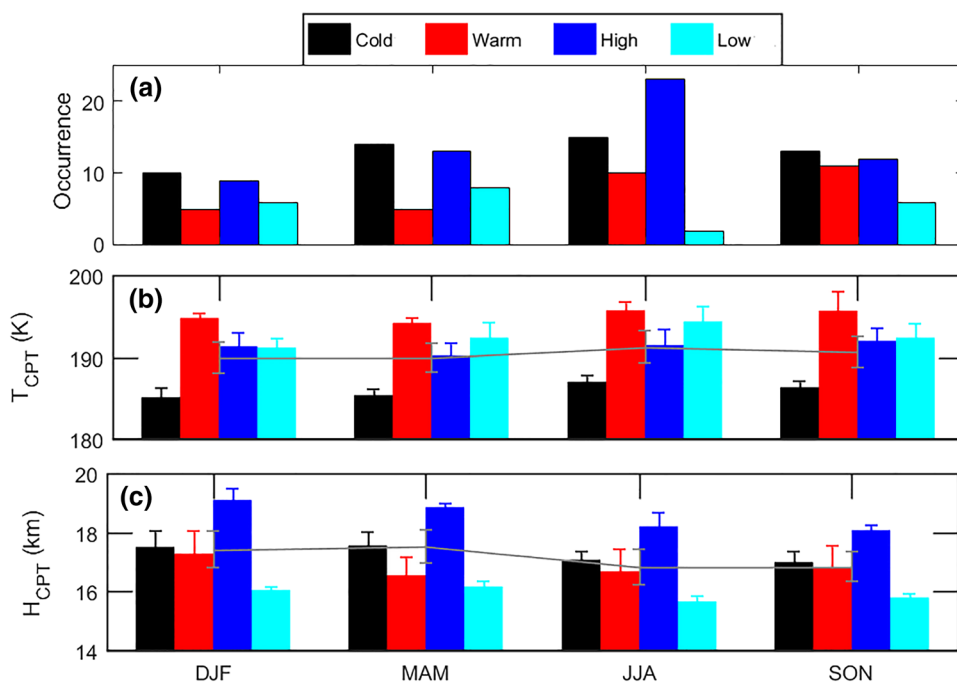
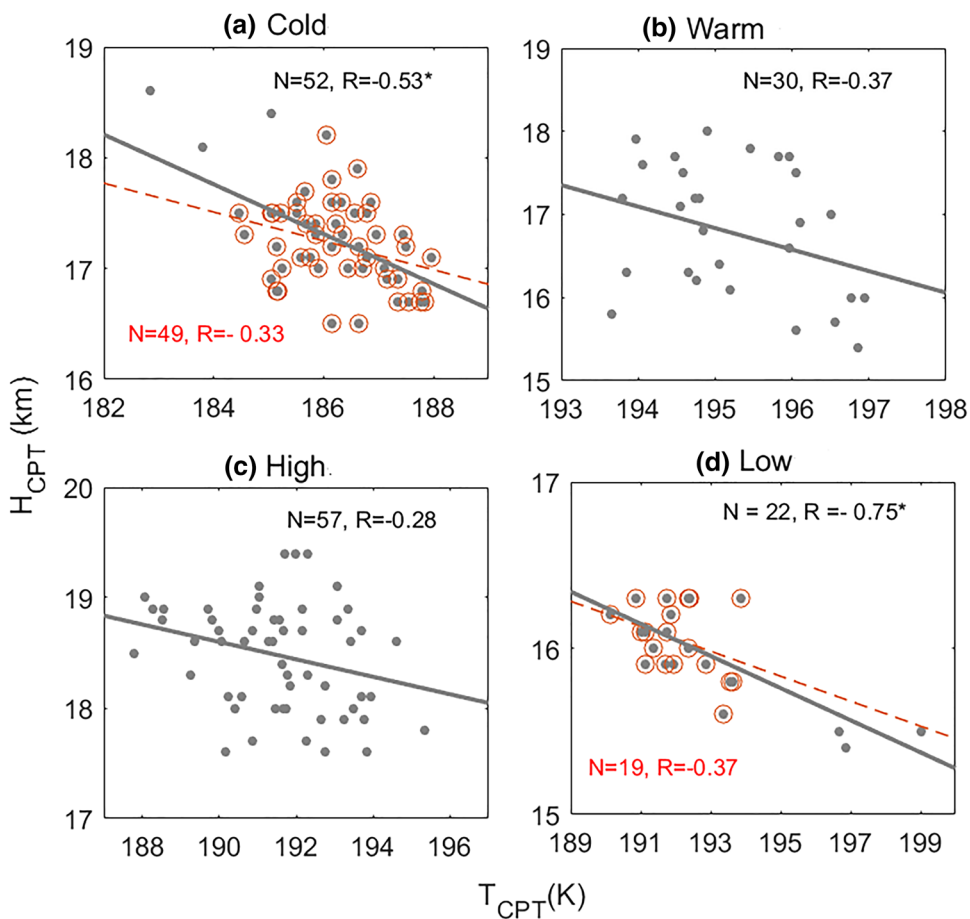


Fig. 6 Scatter plot between H_{CPT} and T_{CPT} for the extremely **a** cold, **b** warm, **c** high, and **d** low cases



are seen to occur at about ~ 18 km several times. It indicates that these extremely warm tropopauses, though occurring

at higher altitudes, need not necessarily be the colder one. The typical warmest tropopause ($H_{CPT} = 16.2$ km,

$T_{\text{CPT}} = 194.8 \text{ K}$) is observed on 23 January 2014 (Supplementary Figure S3b). In general, for the extremely warm tropopause cases, T_{CPT} and H_{CPT} show insignificant anti-correlation ($r = -0.37$).

The seasonal mean H_{CPT} (Fig. 5c) for the extremely high tropopause ranges from $18.1 \pm 0.15 \text{ km}$ (in SON) to $19.17 \pm 0.4 \text{ km}$ (in DJF), and their corresponding mean T_{CPT} (Fig. 5b) varies between $190.6 \pm 1.5 \text{ K}$ (in MAM) and $192.3 \pm 1.3 \text{ K}$ (in SON). The H_{CPT} for the extremely high case is higher by ~ 1.0 – 1.7 km from the climatological mean tropopause. From the scatter plot (Fig. 6c), it can be seen that only a few extremely high tropopauses are colder than 191 K . The typical highest tropopause ($H_{\text{CPT}} = 19.4 \text{ km}$, $T_{\text{CPT}} = 192.3 \text{ K}$) is observed on 02 February 2007. Similar to the extremely warm tropopause cases, T_{CPT} and H_{CPT} for the extremely high tropopause cases are insignificantly anti-correlated ($r = -0.28$). In this case, T_{CPT} has a poor seasonal structure when compared to H_{CPT} .

The seasonal mean H_{CPT} (Fig. 5c) for the extremely low tropopause ranges from $15.5 \pm 0.14 \text{ km}$ (JJA) and $16.19 \pm 0.14 \text{ km}$ (MAM), and their corresponding mean T_{CPT} (Fig. 5b) varies between $191.7 \pm 0.83 \text{ K}$ (in DJF) to $195.1 \pm 2.5 \text{ K}$ (in JJA). The H_{CPT} for the extremely low cases are lower by ~ 1.0 – 1.3 km from the climatological mean tropopause. Though the extremely low tropopauses occur at a lower altitude, T_{CPT} attains lesser than 191 K on several occasions (Fig. 6d). The typical lowest tropopause ($H_{\text{CPT}} = 15.4 \text{ km}$, $T_{\text{CPT}} = 196.9 \text{ K}$) is observed on 26 July 2010 (Supplementary Fig S3d). This typical temperature profile also shows the secondary tropopause ($H_{\text{CPT}} = 17.4 \text{ km}$, $T_{\text{CPT}} = 197 \text{ K}$) $\sim 2 \text{ km}$ above the CPT. Over Gadanki, in general, we have observed that the extremely low tropopauses are associated with double tropopause (Mehta et al. 2011a, b). The T_{CPT} and corresponding H_{CPT} for the extremely low cases is highly anti-correlated ($r = -0.75$), significant at a 95% confidence level (Fig. 6d). Note that if top three extremely low cases (shown encircled) are excluded, T_{CPT} and H_{CPT} for the remaining 19 cases are insignificantly anti-correlated (-0.37).

Thus, the temporal distributions of the extreme tropopauses reveal that they occur independently except for a few. The extremely cold CPT needs not to be the extremely high CPT and vice versa, and the extremely warm CPT needs not to be the extremely low CPT and vice-versa. The poor negative correlation between T_{CPT} and H_{CPT} of the extreme tropopauses indicates that they do not always agree with 'higher and colder' and 'lower and warmer' tropopause characteristics. The month-wise variation of the extremely cold and low tropopauses shows that they are not always higher and colder during NH winter and lower and warmer during NH summer season (Supplementary Fig. S4), resulting in poor anti-correlation between T_{CPT} and H_{CPT} . For the extremely warm cases, T_{CPT} becomes colder and warmer during NH

winter and summer, respectively. However, not the H_{CPT} , which shows uniform variation throughout the year (Supplementary Fig. S4), resulting in insignificant anti-correlation between T_{CPT} and H_{CPT} . Similarly, for the extremely high tropopause case, H_{CPT} is higher and lower during NH winter and summer seasons, respectively. However, T_{CPT} has very poor seasonal variation and appears roughly uniform throughout the year (Supplementary Fig. S4) resulting in insignificant anti-correlation between T_{CPT} and H_{CPT} .

Mehta et al. (2011a, b) have investigated the minimum and maximum CPT altitudes calculated for each grid box using COSMIC GPS RO data and their global distribution over the tropics during different seasons. They observed that the CPT altitude has a large variation ranging from 15 to 19 km . The minimum CPT altitude ranges from 15 – 16.4 km , and the maximum CPT altitude ranges from 17 to 18.6 km . These minimum and maximum CPT altitudes indicate that the frequent occurrence of the extremely low and high tropopauses over the tropical region, respectively.

3.3 Mean thermal structure of the extreme tropopause

We have segregated all the temperature profiles between 12 and 22 km for the extremely cold, warm, high, and low cases and obtained their mean profiles as shown in Fig. 7. We have also shown these extremely cold, warm, high, and low cases on the potential temperature surfaces between 350 and 500 K in the supplementary Fig. S5. The mean temperatures of these extreme cases reveal that their thermal structures are distinct. It is interesting to note that individual extreme temperature profiles under different extreme cases possess similar thermal structures. For the extremely cold cases, the tropopauses are sharper, while the rest of the cases is the border. Again, these broader cases are different among themselves. For the extremely warm tropopause cases, the temperature between $\sim 16 \text{ km}$ and 18.5 km is nearly constant ($\frac{dT}{dz} \cong 0$). For the extremely high tropopause cases, the temperature between $\sim 16 \text{ km}$ and 18.5 km slightly decreases ($\frac{dT}{dz} < 0$). For the extremely low tropopause cases, the temperature increases ($\frac{dT}{dz} > 0$) slowly (i.e., having a very low lapse rate) with an altitude between $\sim 16 \text{ km}$ to 18.5 km (Fig. 7a–d). Figure 7e compares the mean thermal structure of these extreme cases. It reveals a tropopause region bounded by the mean tropopause at $\sim 16 \text{ km}$ (as the lower boundary) and the mean tropopause at $\sim 18.5 \text{ km}$ (as the upper boundary) i.e., the between the potential surface $\sim 363 \text{ K}$ to 403 K , respectively. The mean tropopause height obtained from the individual profiles for different extreme cases varies from $\sim 16 \text{ km}$ to $\sim 18.5 \text{ km}$. Note that the mean tropopause obtained from the individual profiles does not precisely coincide with calculated from mean

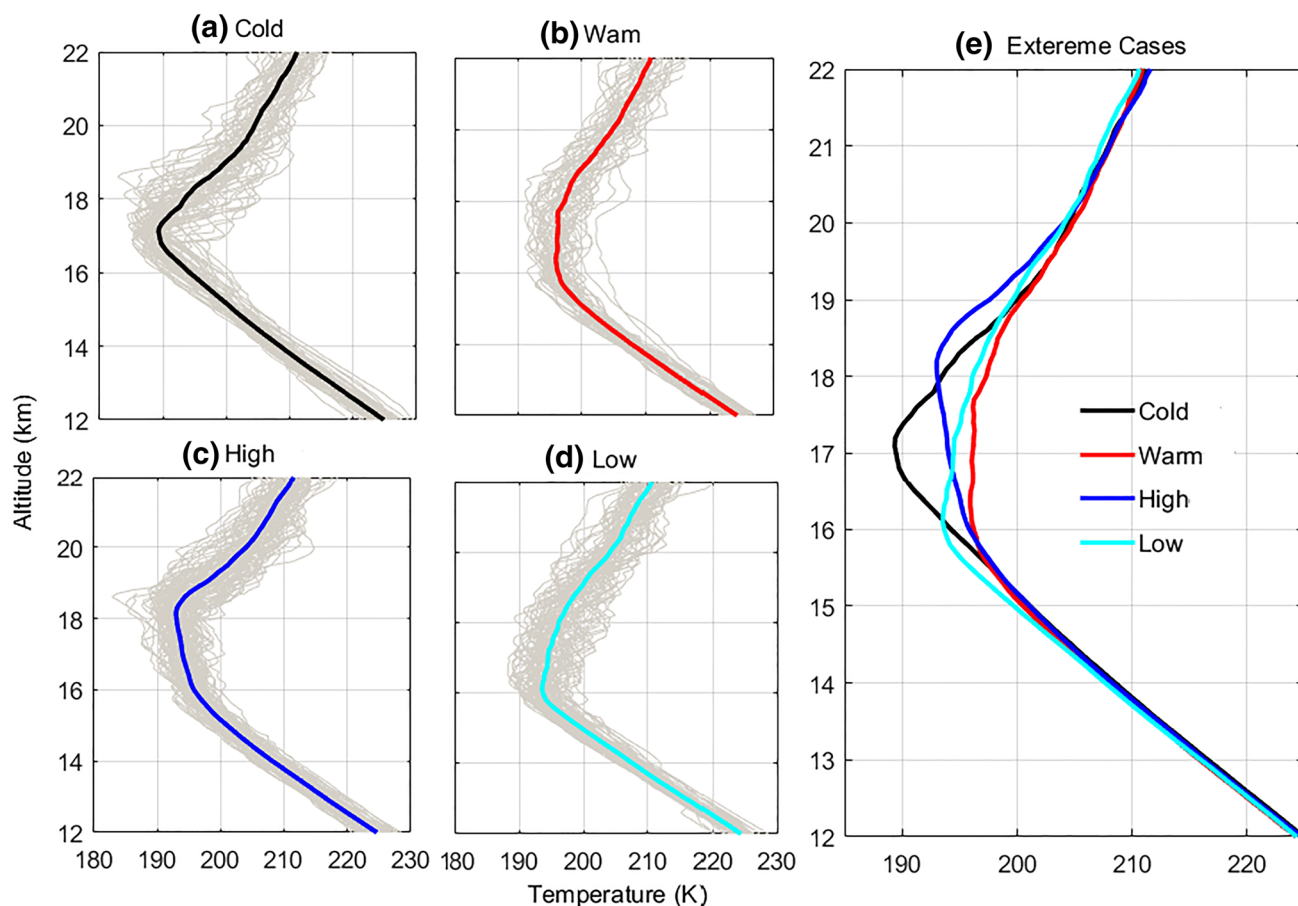


Fig. 7 All individual and their mean temperature profiles were observed for the extremely **a** cold, **b** warm, **c** high, and **d** low. **e** Represents the thermal structure for different extreme cases

temperature profiles. In this bounded region between 16.0 km and 18.5 km, large perturbations in thermal structure mainly account for these well-defined extreme temperature profiles. Whose occurrence results in a significant day-to-day variation in the tropical tropopause. It can be noticed that different extreme tropopause temperature profiles about one km below and above the bounded region represent nearly the same mean structure.

Supplementary Fig. S6 presents the mean and standard deviation (SD) of the temperature, height, and sharpness for the extremely cold, warm, high, and low tropopause cases. Note that tropopause sharpness is defined as the change in static stability across the CPT (Detailed in Supplementary material). As mentioned earlier, the cold tropopause means the T_{CPT} is $\sim 186.1 \pm 1.1$ K, much colder than the threshold T_{CPT} (191 K) required for the freeze-drying of air enters into the lower stratosphere. Such extremely cold tropopause would result in the extreme dryness of the lower stratosphere, as initially explained by Dobson et al. (1946) and Brewer (1949). However, the extremely cold tropopause heights (17.30 ± 0.47 km) occur nearly at the same altitude

of the NH winter tropopause (17.5 ± 0.5 km) is commonly formed. Figure S5c shows that these extremely cold tropopauses are generally sharper ($7.83 \pm 1.73 \times 10^{-4} \text{ s}^{-2}$). Note that the extremely warm, high and low tropopauses usually are broader as mentioned earlier.

3.4 Ozone and water vapor variability during extreme days

In a case study, Takashima et al. (2010) observed extremely low temperatures near the tropical tropopause associated with the minimum water vapor and higher frequency of cirrus clouds occurrence. The annual minimum for tropopause height in July and August is accompanied by the extremely warm tropopause temperatures, which implies higher saturation mixing ratios for water vapor and higher temperature thresholds to form ice particles during this season. To understand the role of the ozone and water vapor on the extreme tropopauses, we have collected the MLS data closest to the Gadanki for the extreme cases during 2006–2014. In total,

26 ozone and water vapor profiles are obtained on extreme tropopause cases.

Figure 8 shows all the water vapor profiles and their corresponding means between altitudes 13 and 20 km for the extremely cold, warm, high and low tropopause cases. It is interesting to notice that the vertical structures of the water vapor for each extreme tropopause case are similar. These extreme cases have similar vertical structures though they show large variability. The mean extreme water vapor profiles indicate the minimum value for the extremely cold tropopause cases and the maximum value for the extremely warm tropopause cases between the altitudes 15–17 km. The water vapor profiles for these extremely cold, warm, high, and low cases are also shown on the potential temperature surfaces between 360 and 450 K in the supplementary Fig. S7. The water vapors at 16.2 km (~ 100 hPa) are 2.7, 4.6, 3.5, and 3.6 ppmv for the extremely cold, warm, high, and low tropopause cases, respectively.

Figure 9 shows all the ozone profiles and their corresponding mean between the altitudes 13–20 km for the

extremely cold, warm, high, and low tropopauses. The ozone profiles for these extremely cold, warm, high, and low cases are also shown on the potential temperature surfaces between 360 and 450 K in the supplementary Figure S8. Although we have a very limited number of ozone observations, the distinct structure of ozone profiles suggests that ozone plays a significant role in the occurrence of the extreme tropopause and its day-to-day variability. It is well known that the ozone absorbs UV radiation and radiatively warms the stratosphere. As expected, for the extremely warm tropopause cases, ozone concentrations are found to be more when compared to the extremely cold tropopause. It means that the extremely warm tropopause occurs with high ozone concentrations in the lower stratosphere, while the extremely cold tropopause occurs with low ozone concentrations in the lower stratosphere. The inset picture shows the variability of the ozone peak with extreme tropopause cases. It is interesting to observe the higher ozone concentrations for the extremely warm and high tropopauses when compared to the extremely cold

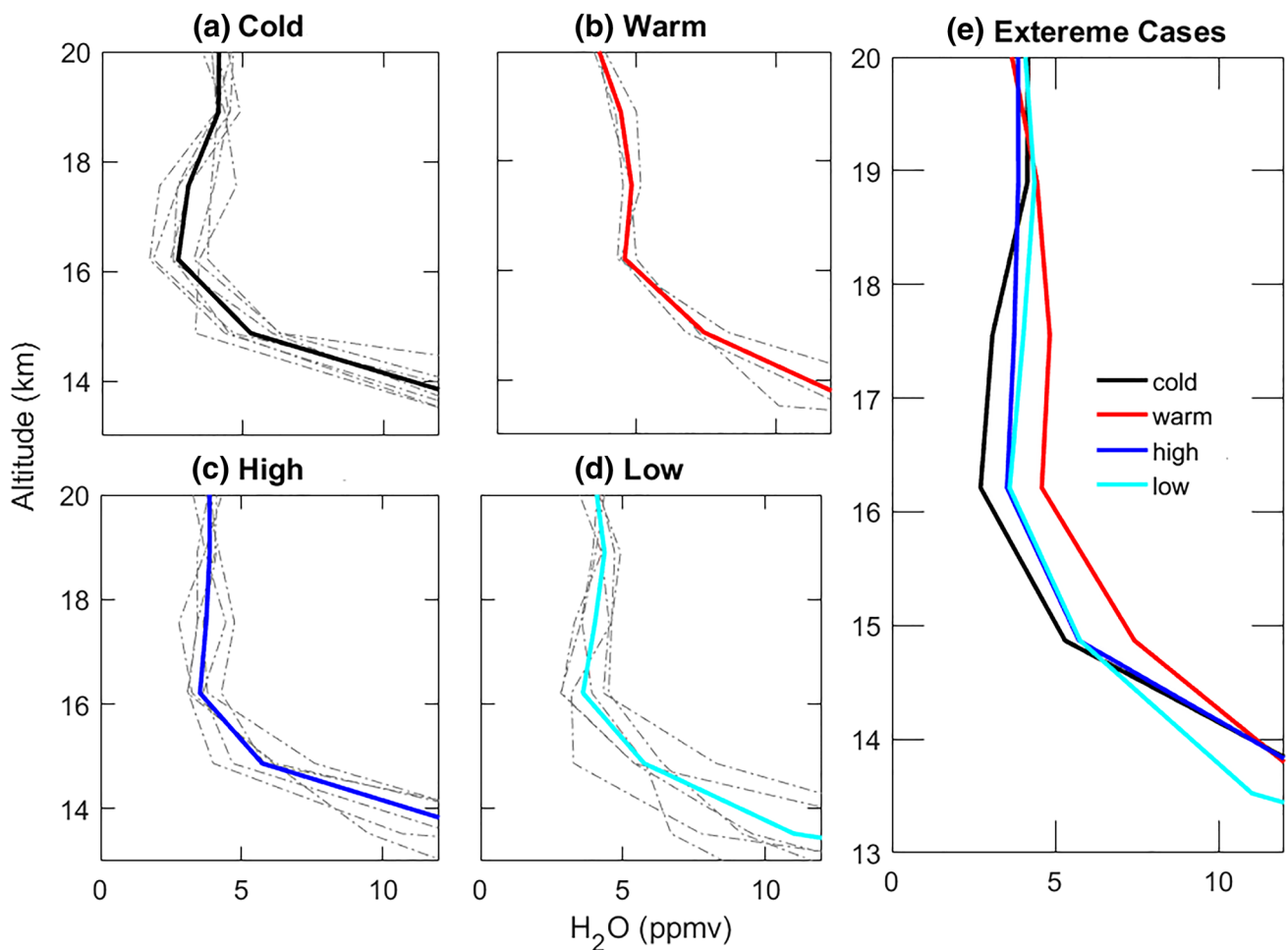


Fig. 8 Same as Fig. 7 but for water vapor profiles between the altitudes 13–20 km

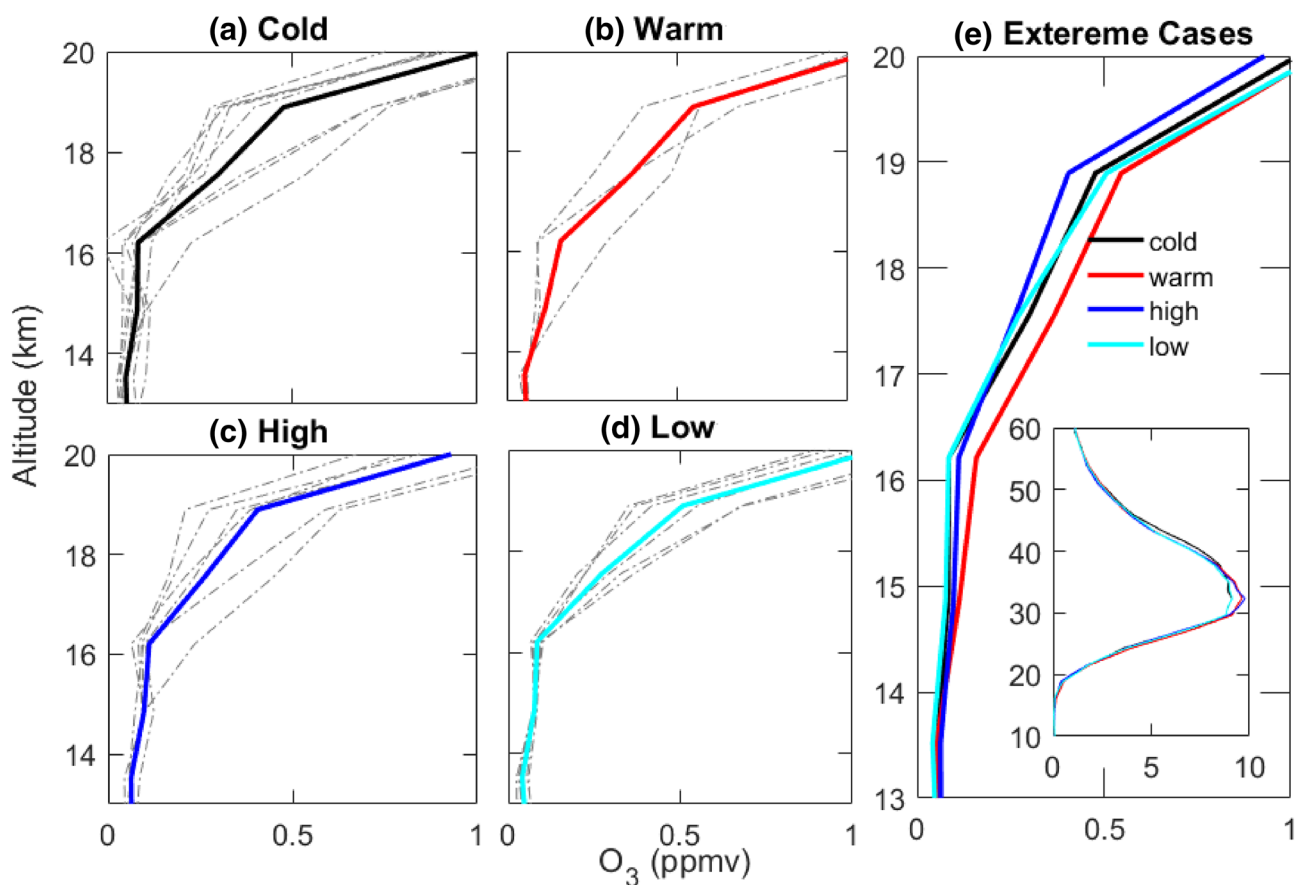


Fig. 9 Same as Fig. 7 but observed for ozone profile between the altitudes 13–20 km

and low tropopauses. The possible link between extreme tropopauses and ozone peak variability cannot entirely be ascertained with this limited dataset and needs to be investigated in detail.

3.5 Role of potential vorticity (PV) intrusion

Atmospheric Rossby waves are generated due to variation in the Coriolis force with latitude and to conserve the absolute vorticity (Holton 1992). It plays an important role in transferring the hot air from tropics towards poleward and cold air towards equatorward. At the critical amplitude of the wave, crest or trough of the wave overturns resulting to the Rossby waves breaking and hence distortion in the PV contours (McIntyre and Palmer 1983; Norton 1994). These PV contours extends deep equatorward or poleward leading to stratosphere-troposphere exchange (Holton et al. 1995). Several studies have shown the association between the Rossby wave breaking with the isentropic transport of extra-tropical air masses and trace gases such as ozone in the UTLS (Appenzeller et al. 1996; Jing et al. 2004). Thus, mixing of the air masses from different boundaries may lead to the variation of

the in T_{CPT} and H_{CPT} . To understand the influence of the Rossby waves breaking, we have analyzed the PV at the isentropic levels 330, 350 and 370 K for all the extreme cases. There were several PV intrusions due to the Rossby wave breaking on the extreme tropopause cases, however, the intrusion extending to Gadanki was only observed on 10 April 2008 for the extremely cold case, and on 29 March 2009 and 31 March 2021 for extremely high cases. Figure 10 shows the PV intrusions at 350 K for 10 April 2008 and 31 March 2012 along with the temperature profiles at 17:30 IST observed over Gadanki. On 10 April 2008, the tropopause is found to be extremely cold ($T_{CPT} \sim 186.2$ K) indicating the intrusion of the cold extratropical air with PV values greater than 1.5 PVU ($\sim 1 \text{ PVU} = 10^{-6} \text{ km}^2 \text{ kg}^{-1} \text{ s}^{-1}$) equatorward to Gadanki. However, on 31 March 2012, tropopause is extremely high ($H_{CPT} \sim 18.8$ km) with $T_{CPT} \sim 193$ K. In this case, the tropopause is broad and warmer than the previous case. As the intrusion brings both cold extratropical air and ozone, the different effect on the tropopause for these two cases depend upon the relative roles played by the cooling of the extratropical air mass and radiative warming by ozone. We have juxtaposed the extreme tropopauses

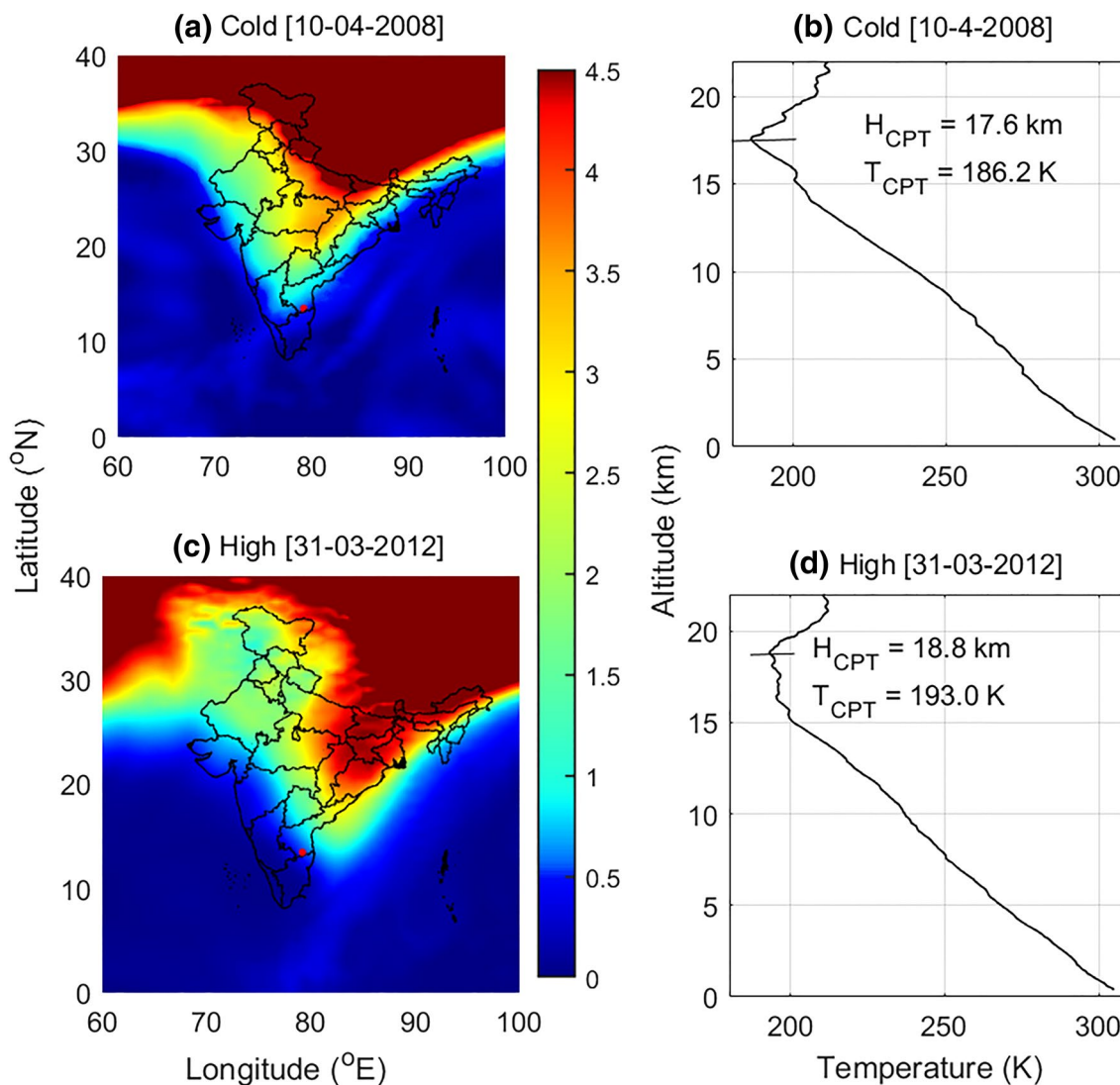


Fig. 10 **a** Typical longitude-latitude section of the PV intrusion at the isentropic surface 350 K during for the extremely cold tropopause case and **b** the temperature profile between 0 and 22 km observed on 10 April 2008 over Gadanki. **c**, **d** are same as **(a, b)** for the extremely

high tropopause case observed on 31 March 2008. H_{CPT} and T_{CPT} are also shown in **(b)** and **(d)**. Color bar indicates the PV values in PVU ($\sim 1 \text{ PVU} = 10^{-6} \text{ km}^2 \text{ kg}^{-1} \text{ s}^{-1}$)

over the time-height section of the PV between altitudes 14–20 km for 2006–2014 shown in supplementary Fig. S9. It can be seen that PV shows a large day to day variability of 1.5 PVU surfaces. To understand further, we have segregated all the PV profiles between 13 and 22 km for the extremely cold, warm, high, and low tropopause cases and obtained their mean profiles as shown in Fig. 11. Interestingly, the mean PV profiles also show significant difference between the extremely cold and warm tropopause cases with higher PVU for the latter case as observed for the temperature and tracers (water vapor and ozone) (Figs. 7, 8, 9). It indicates that extremely warm

tropopause cases are associated with ozone rich air that could have either resulted due to PV intrusion or subsidence arises due to deep convection.

3.6 Role of convection

It is well known that convection plays an important role in modifying the tropical tropopause structure (Muhsin et al. 2018; Sherwood et al. 2003). Muhsin et al. (2018) have examined the role of the different types of convection on the variation of the tropical tropopause parameters over Gandaki and reported that H_{CPT} lowers with the increase in

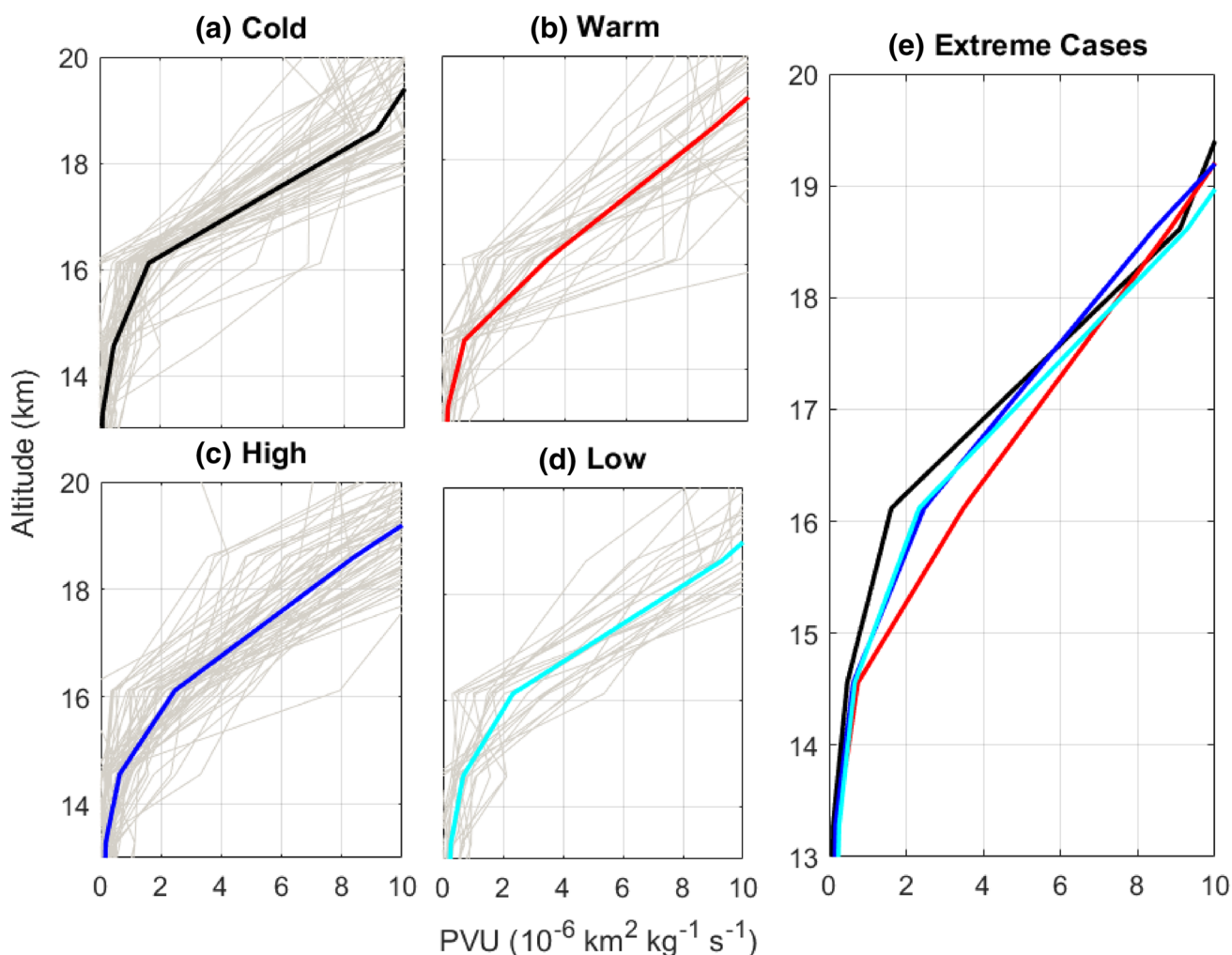


Fig. 11 Same as Fig. 7 but observed for potential vorticity (PV) profile between the altitudes 13–20 km

convective strength from shallow to deep convection. We also performed a similar analysis to examine the role of convection on the occurrence of the extreme tropopauses following Meenu et al. (2010). All the extreme tropopauses and the corresponding temperature profiles are segregated based on the different types of convective clouds occurring at different altitudes using the IRBT data over 2006–2014. $IRBT > 280$ K corresponds to convective cloud top altitude (H_{CCT}) < 2 km for the clear sky conditions. For convective clouds ($H_{CCT} > 2$ km), the IRBT thresholds are considered as (i) 280–270 K corresponding to $H_{CCT} = 2$ –5 km, (ii) 270–245 K corresponding to $H_{CCT} = 5$ –8 km (iii) 245–235 K corresponding to $H_{CCT} = 8$ –10 km, (iv) 235–220 K corresponding to $H_{CCT} = 10$ –12 km, and (v) < 220 K corresponding to $H_{CCT} > 12$ km.

Figure 12a shows the distributions of the clear sky and convective days for the extreme tropopause cases. Out of 161 extreme cases, 71 cases fall under clear sky days while 90 cases for the convective days. Out of 90 convective cases,

30, 51, 8, and 1 cases are observed for $H_{CCT} = 2$ –5 km, 5–8 km, 8–10 km, and 10–12 km. Figures 12b, c show the mean and standard deviation of the T_{CPT} and H_{CPT} for the clear sky ($H_{CCT} < 2$ km) and convective ($H_{CCT} = 2$ –5 km, and $H_{CCT} = 5$ –8 km) cases. Other convective cases have an inadequate number of observations for different extreme cases, and hence they are not analyzed further. Out of 30 (51) $H_{CCT} = 2$ –5 km ($H_{CCT} = 5$ –8 km) cases, 11 (21), 7(9), 9(15), and 3(7) are observed for the extremely cold, warm, high and low tropopauses, respectively. Under very shallow convective clouds ($H_{CCT} = 2$ –5 km), extreme T_{CPT} does not show any significant change relative to clear sky T_{CPT} . However, H_{CPT} for the extremely cold, warm, and high tropopauses lower for very shallow convective clouds when compared to clear sky H_{CPT} . For the extremely low tropopause, H_{CPT} for very shallow convective clouds becomes higher relative to clear sky H_{CPT} . For the shallow convective clouds ($H_{CCT} = 5$ –8 km), the extremely cold tropopause becomes warmer by ~ 1.5 K and lower by ~ 0.5 km relative

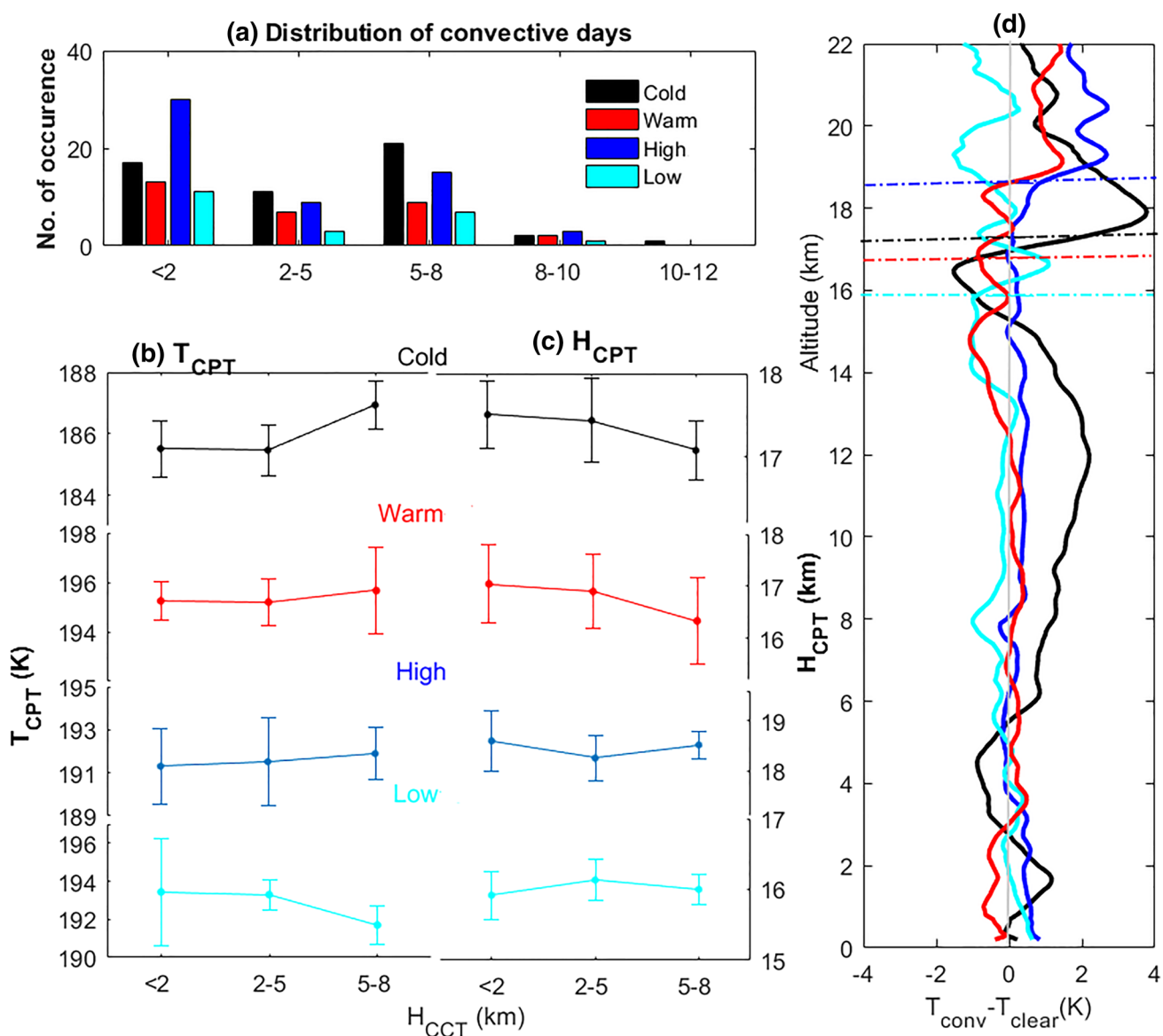


Fig. 12 **a** Distribution of the occurrence of the extreme tropopauses for the clear sky (<2 km) and convective clouds with the top between 2 and 5 km, 5 and 8 km, 8 and 10 km, and 10–12 km. **b**, **c** The mean and one standard deviation of the T_{CPT} and H_{CPT} for the extreme tropopause under the clear sky, convective clouds with the top between 2

and 5 km and 5 and 8 km. **d** Vertical profiles of temperature anomaly (subtracted by clear sky temperature profiles) of convective top between 5 and 8 km. Horizontal dashed lines indicate the H_{CPT} for the respective extreme tropopauses

to clear sky condition. While the T_{CPT} remains unchanged and H_{CPT} lowers by 0.7 km for the extremely warm cases, both T_{CPT} and H_{CPT} remain unchanged for the extremely high cases, and T_{CPT} becomes colder by ~1.7 K, and H_{CPT} remains unchanged for the extremely low cases relative to clear sky condition.

Figure 12d shows the difference between the shallow convective temperature profiles and the clear sky temperature profiles. We observed prominent warming of ~2 K between 8 and 14 km (above the cloud top), cooling of ~2 K just below the CPT (in the tropical tropopause layer), and

warming of ~4 K at ~18 km just above the CPT (in the lower stratosphere) for the extremely cold tropopause cases. For the extremely warm and high tropopause cases, warming is also observed above the cloud top in the mid-troposphere, however with smaller magnitudes and lesser vertical extent when compared to the extremely cold tropopause cases. Cooling (warming) below (above) the CPT for the extremely warm tropopause and warming above the CPT for the extremely high tropopause cases are also observed; however not pronounced as the extremely cold tropopause cases. For the extremely low tropopauses, such a feature was

not observed. In general, though these extreme cases tend to behave in a similar way, there are some deviations, which we would like to carry out as a separate study in the future. The anomalous warming above the cloud top is known due to the latent heat release from convective clouds (Houze Jr 2004) as a direct response of convection, while anomalous cooling (warming) just below (above) CPT could be an indirect response to convection (Gettelman and Birner 2007; Johnson and Kriete 1982; Muhsin et al. 2018; Paulik and Birner 2012; Randel et al. 2003). The extreme tropopause temperature profiles show cooling below the CPT within the tropical tropopause layer region (Kim and Dessler 2004), which could be either due to convective detrainment and turbulent mixing (Sherwood et al. 2003) or due to radiative cooling caused by reduction of longwave radiation (Webster and Stephens 1980).

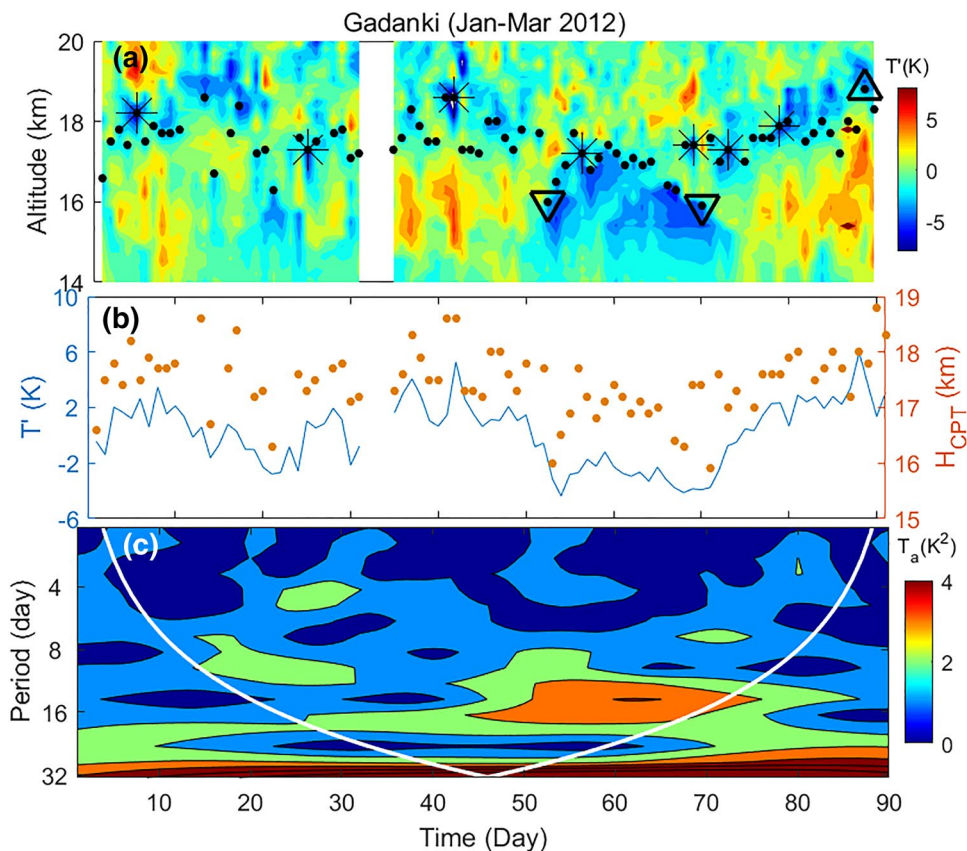
3.7 Role of equatorial wave in the extreme variability

Equatorial wave propagations in the tropopause region significantly modulate the tropical tropopause structure (Boehm and Verlinde 2000; Munchak and Pan 2014; Tsuda et al. 1994). These waves can modulate the T_{CPT} up to 8 K and H_{CPT} up to its vertical wavelength ~ 4 km (Boehm and Verlinde 2000), which causes the tropopause to vary extremely.

Several times extreme tropopause is associated with warm and cold temperature anomalies, as mentioned in Fig. 4. The role of the equatorial wave on the extreme variation of the tropopause is demonstrated by taking one such event of temperature anomalies associated with the occurrence of the extremely cold and low CPT observed during January–March 2012, as shown in Fig. 13.

During this period, the H_{CPT} shows a sinusoidal pattern indicating wave propagation. Seven cold tropopause cases occurred during this period. Among them, extremely cold tropopause with $T_{\text{CPT}} \sim 182.8$ K and $H_{\text{CPT}} \sim 18.6$ km is observed on 11 February 2012 (See Supplement Fig S3a). It is known that Kelvin wave amplitudes maximize near the tropopause, which can sometimes lead to the formation of the extremely cold tropopause (Ratnam et al. 2006). The downward shift in the temperature anomalies and H_{CPT} can be noticed, particularly on the 2nd week of February to March 2012, indicating the influence of downward phase propagating waves. In order to examine the role of equatorial planetary-scale waves, the time series of temperature averaged between 16 and 17 km is subjected to spectral analyses (Morlet wavelet) to obtain the dominant wave periods and the times of their occurrences. For this analysis, we have obtained the temperature perturbations by subtracting the mean temperature profile over January–March from individual temperature profiles and subjected it to wavelet analysis.

Fig. 13 **a** Time height section of the contour plot of the temperature anomalies during January to March 2012 superimposed with H_{CPT} . **b** Time series of temperature anomalies averaged between 16 and 17 km and H_{CPT} . **c** Wavelet spectrum of temperature (in terms of power) at 16–17 km from January to March 2012. The white curve in (c) represents the cone of influence



It is seen that waves with periods 10–20 days are significant from 15 February to 10 March 2012. The dominant periods within the cone of influence are only considered to avoid edge effects. To ascertain the nature of these waves, the amplitude and phase of the dominant wave periods of 10-days in temperature and zonal wind during January–March 2012 are obtained as shown in Supplementary Figure S10. It is observed that the amplitudes in temperature and zonal wind in the altitude range 15–20 km are ~ 1.0 K and 2–3 m/s, respectively (Figure S10a). The phase shows clear downward propagation (upward propagating wave) with temperature phase leading to the zonal wind phase indicating the Kelvin wave propagation (Figure S10b) (Mehta et al. 2013). Thus, the Kelvin wave can sometimes modify the tropopause structure significantly, resulting in the extremely cold tropopause. Such extremely cold tropopause may occur due to the vertically propagating Kelvin wave (Tsuda et al. 1994).

4 Discussions

The high-resolution GPS radiosonde observations over the Indian monsoon region (Gadanki) are utilized to demonstrate the extreme variability of the tropical tropopause. CPT shows high-frequency variabilities within the season, which are mainly known to be due to day-to-day weather fluctuations, planetary wave activities, and stratosphere-troposphere exchange processes (Holton et al. 1995; Mehta et al. 2010; Tsuda et al. 1994). The one sigma variation of the T_{CPT} (H_{CPT}) is ~ 2.0 K (0.66 km) over Gadanki; however, T_{CPT} (H_{CPT}) becomes extremely cold or warm (high or low) by ~ 4 K (~ 1.32 km) from its monthly mean temperatures in a significant number of times. The long-term radiosonde observations enable us to identify a sufficient number of extreme tropopause cases, defined as the cases falling outside the two-sigma level of climatological mean tropopause over 2006–2014. Over Gadanki, the probability distributions of the T_{CPT} and H_{CPT} are nearly Gaussian. The extremely cold (warm) tropopause is defined as the T_{CPT} is lesser (greater) than the lower (upper) limit of its two-sigma level. Whereas the extremely high (low) tropopause is defined as the H_{CPT} is greater (lesser) than the upper (lower) limit of its two-sigma level. The extreme tropopause cases are about 5% (161) of the total data over 2006–2014. Out of which 52, 30, 57, and 22 cases are the extremely cold, warm, high and low tropopauses, respectively.

On a seasonal scale, the tropical tropopause is colder and higher during the NH winter and warmer and lower tropopause during the NH summer (Seidel et al., 2001). However, our findings demonstrate that the extremely cold and high (warm and low) tropopauses occur throughout the year and not only during the NH winter (summer) season.

The extremely cold and high tropopause is more frequent during the NH summer and not during the NH winter due to the frequent occurrence of deep convection during the former season (Newell and Gould-Stewart, 1981). These extreme cases occur independently; that is, the extremely cold (warm) one need not necessarily be the high (low) and vice versa. Our observations also show that these extreme tropopause cases have a unique vertical structure. The distinct thermal structures of the mean temperature profiles of these extreme cases reveal that the extremely cold tropopause is sharper. In contrast, the extremely warm, high, and low tropopauses are border. They are characterized as unique lapse rates between ~ 16 km to 18.5 km, nearly equal to zero, greater than zero, and lesser than zero, respectively.

The plausible mechanisms for the extreme tropopause cases are deep convection, propagation of the equatorial wave, stratosphere-troposphere exchange processes, and the formation of the cirrus clouds. Extreme variations in the tropopause altitude may directly bear on the energy source for the stratospheric motions, the exchange of water vapor and ozone between troposphere and stratosphere (Holton 1982). Our observations suggest that the extremely warm tropopause cases are associated with higher water vapor and ozone concentrations when compared to the extremely cold tropopause cases indicating the importance of their radiative effects on the extreme tropopause cases. However, the role of radiative effects on the temperature and the tropopause variation due to water vapor and ozone are not easy to quantify as they are associated with deep convection events. It is well known that the transport of the tropospheric water vapor into the UTLS and the intrusion of the ozone-rich air into the upper troposphere are mainly associated with the deep convection events. The transport of the extratropical cold air-mass and ozone are also associated with PV intrusions that play relative roles on the UTLS temperature. Our observations show that the PV values for the extremely warm tropopause cases are associated with higher PVU when compared to the extremely cold tropopause cases. It indicates that PV intrusions also play an important role on the occurrence of the extreme tropopause cases. A detailed investigation extreme cases over the entire tropics will provide the better understanding towards its association with PV intrusions which we are planning to carry out in a future study.

The role of convection on the tropical tropopause is well known, and it is found that H_{CPT} lowers with an increase in convective strength from shallow to deep convection (Muh-sin et al. 2018). Under the shallow convection, extreme temperature profiles, in general, show prominent warming (~ 2 K) between 8 and 14 km due to the latent heat release from convective clouds as a direct response of convection while anomalous cooling (~ 2 K) just below the CPT and warming (~ 4 K) just above the CPT could be an indirect response to convection (Johnson and Kriete 1982; Randel

and Wu 2003). Over the period 2006–2014, two tropical cyclones had passed through Gadanki: Thane during 25–31 October 2011 and Nilam during 28 October–01 November 2012 (Das et al. 2016; Venkat Ratnam et al. 2016). During the Nilam cyclone, the extremely cold T_{CPT} (~ 186 K) was observed on 31 October 2012 over Gadanki.

In-situ generated tropopause cirrus clouds form due to homogeneous nucleation of ice crystals at extremely cold temperature of -70 °C to -90 °C near the CPT (Cziczo and Froyd 2014). Over Gadanki, Ali et al. (2020) observed that tropopause cirrus warms the CPT by ~ 1.2 K, indicating that the extreme tropopause may also result from radiative effects from the cirrus clouds (Fu et al. 2018; Hartmann et al. 2001). Following Ali et al. (2020), simultaneous observations of the radiosonde and CALIPSO are obtained found the two, one, two, and three cases for the extremely cold, warm, high, and low tropopauses, respectively, in the presence of the cirrus clouds. Such coincidence indicates that extreme tropopauses especially extremely cold tropopause may sometimes result due to radiative effects of the cirrus clouds. Finally, we examined the role of the equatorial wave and found that they can modify the tropopause structure significantly, leading to the formations of the extreme tropopauses.

5 Summary and conclusions

In this paper, extreme variabilities of the tropical tropopause are identified, and the roles of convection, PV intrusions, planetary wave activities, and water vapor and ozone mixing ratios are examined using radiosonde, IRBT, MLS, and PV data sets over Gadanki. The main findings on the extreme variability of the tropical tropopause are summarized below.

1. The probability distribution of the T_{CPT} and H_{CPT} follow nearly Gaussian curve, which indicates that 5% of the total data behaves extremely with $T_{\text{CPT}} < 188.5$ K, $T_{\text{CPT}} > 195.9$ K, $H_{\text{CPT}} < 16.5$ km, and $H_{\text{CPT}} > 17.6$ km, defined as the extremely cold, warm, low and high tropopause, respectively.
2. The extreme tropopauses are distributed throughout the year and occur randomly in all the seasons. The extremely cold and high tropopauses occur independently. Similarly, the extremely warm and low tropopauses also occur independently except for a few cases.
3. The extremely cold, warm, and high tropopauses occur more frequently during NH summer than NH winter. In contrast, the extremely low tropopause occurs more frequently during NH winter and spring than NH summer.
4. The T_{CPT} and H_{CPT} for the extreme cases show nearly similar seasonal variation as the climatological mean T_{CPT} and H_{CPT} , respectively. The extremely cold (warm)

- tropopause is colder (warmer) by about 4–5 K from the climatological mean tropopause. The extremely high (low) tropopause is higher (lower) by ~ 1.0 – 1.7 km (~ 1.0 – 1.3 km) from the climatological mean tropopause.
5. The mean temperature profiles of the extremely cold, warm, high, and low tropopauses possess distinct thermal structures between the altitudes ~ 16.5 – 18 km. For the extremely cold cases, the tropopauses are sharper, while the other cases are the border. These broader tropopauses cases are different among themselves. For the extremely warm, high, and low tropopause cases, the temperature between ~ 16 km to 18.5 km is nearly constant ($\frac{dT}{dz} \cong 0$), slightly decreases ($\frac{dT}{dz} < 0$) and gradually increases ($\frac{dT}{dz} > 0$), respectively.
 6. The water vapor profiles and their corresponding mean between the altitudes 13–20 km for each extreme tropopause case are similar and showing a large variability with maximum (minimum) water vapor for the extremely warm (cold) tropopause cases. Ozone concentrations for the extremely warm tropopauses are found to be more when compared to the extremely cold tropopauses. Similarly, higher PVU are observed for the extremely warm tropopause cases when compared to the extremely cold tropopause cases.
 7. Convection plays an important role in the extreme variability of the tropopause, especially for the extremely cold tropopause. Under the shallow convective clouds ($H_{\text{CCT}} = 5$ – 8 km), the extremely cold tropopause becomes warmer by ~ 1.5 K and lower by ~ 0.5 km relative to clear sky conditions.

Supplementary Information The online version contains supplementary material available at <https://doi.org/10.1007/s00382-022-06264-7>.

Acknowledgements This work is fully supported by the Department of Science and Technology, Government of India – Science and Engineering Research Board (DST-SERB) project (EMR/2015/000525). SKM wishes to thank Director NARL, Gadanki for providing the radiosonde data. VA wishes to thank SRMIST to carry out the research work using the HPCC computational facility. We thank NASA GES DISC for providing Aura-MLS and IRBT data (<https://disc.gsfc.nasa.gov/datasets>) and ECMWF for providing ERA5 data.

Funding Department of Science and Technology, Government of India – Science and Engineering Research Board (DST-SERB) project (EMR/2015/000525).

Data availability The radiosonde data used in this study are available from the dropdown “View & Download Data” listed on the “Data/Experiment” tab of the NARL website (<https://www.narl.gov.in>). MLS and IRBT data can be obtained from NASA Goddard Earth Sciences Data and Information Services Center (GES DISC) (<https://disc.gsfc.nasa.gov/datasets>). ERA5 data can be downloaded from the ECMWF website (<https://www.ecmwf.int/en/forecasts/datasets/reanalysis-datasets/era5>). Data used in this study can be provided upon request to the corresponding author.

Declarations

Conflict of interest The authors declare that they have no known competing financial interests or personal relationships that could have appeared to influence the work reported in this paper.

References

- Ali S, Mehta SK, Annamalai V, Ananthavel A, Reddy R (2020) Qualitative observations of the cirrus clouds effect on the thermal structure of the tropical tropopause. *J Atmos Sol Terr Phys* 211:105440
- Añel JA, Antuña JC, de la Torre L, Castanheira JM, Gimeno L (2008) Climatological features of global multiple tropopause events. *J Geophys Res Atmos*. <https://doi.org/10.1029/2007JD009697>
- Appenzeller C, Davies HC, Norton WA (1996) Fragmentation of stratospheric intrusions. *J Geophys Res* 101:1435–1456. <https://doi.org/10.1029/95JD02674>
- Bhat G (2003) Some salient features of the atmosphere observed over the north Bay of Bengal during BOBMEX. *J Earth Syst Sci* 112:131–146
- Biondi R, Randel W, Ho S-P, Neubert T, Syndergaard S (2012) Thermal structure of intense convective clouds derived from GPS radio occultations. *Atmos Chem Phys* 12:5309–5318
- Boehm MT, Verlinde J (2000) Stratospheric influence on upper tropospheric tropical cirrus. *Geophys Res Lett* 27:3209–3212
- Borsche M, Kirchengast G, Foelsche U (2007) Tropical tropopause climatology as observed with radio occultation measurements from CHAMP compared to ECMWF and NCEP analyses. *Geophys Res Lett*. <https://doi.org/10.1029/2006GL027918>
- Brewer A (1949) Evidence for a world circulation provided by the measurements of helium and water vapour distribution in the stratosphere. *Q J R Meteorol Soc* 75:351–363
- Cziczo DJ, Froyd KD (2014) Sampling the composition of cirrus ice residuals. *Atmos Res* 142:15–31
- Danielsen EF (1982) A dehydration mechanism for the stratosphere. *Geophys Res Lett* 9:605–608
- Das SS et al (2016) Stratospheric intrusion into the troposphere during the tropical cyclone Nilam (2012). *Q J R Meteorol Soc* 142:2168–2179
- Dixon DA et al (2012) An ice-core proxy for northerly air mass incursions into West Antarctica. *Int J Climatol* 32:1455–1465
- Dobson G, Brewer A, Cwiling B (1946) Meteorology of the lower stratosphere. *Proc R Soc Med* 185:144
- Fu Q, Smith M, Yang Q (2018) The impact of cloud radiative effects on the tropical tropopause layer temperatures. *Atmosphere* 9:377
- Fueglistaler S, Haynes P (2005) Control of interannual and longer-term variability of stratospheric water vapor. *J Geophys Res*. <https://doi.org/10.1029/2005JD006019>
- Fueglistaler S et al (2009) Tropical tropopause layer. *Rev Geophys*. <https://doi.org/10.1029/2008RG000267>
- Gottelman A, Birner T (2007) Insights into tropical tropopause layer processes using global models. *J Geophys Res*. <https://doi.org/10.1029/2007JD008945>
- Gottelman A et al (2010) Multimodel assessment of the upper troposphere and lower stratosphere: tropics and global trends. *J Geophys Res*. <https://doi.org/10.1029/2009JD013638>
- Hartmann DL, Holton JR, Fu Q (2001) The heat balance of the tropical tropopause, cirrus, and stratospheric dehydration. *Geophys Res Lett* 28:1969–1972
- Hersbach H, Bell B, Berrisford P, Hirahara S, Horányi A, Muñoz-Sabater J, Thépaut JN (2020) The ERA5 global reanalysis. *Q J R Meteorol Soc* 146(730):1999–2049
- Highwood E, Hoskins B (1998) The tropical tropopause. *Q J R Meteorol Soc* 124:1579–1604
- Holton JR (1982) The role of gravity wave induced drag and diffusion in the momentum budget of the mesosphere. *J Atmos Sci* 39:791–799
- Holton JR (1992) An introduction to dynamic meteorology, 3rd edn. Academic Press, San Diego
- Holton JR et al (1995) Stratosphere-troposphere exchange. *Rev Geophys* 33:403–439
- Houze RA Jr (2004) Mesoscale convective systems. *Rev Geophys*. <https://doi.org/10.1029/2004RG000150>
- Jain A, Das SS, Mandal TK, Mitra A (2006) Observations of extremely low tropopause temperature over the Indian tropical region during monsoon and postmonsoon months: possible implications. *J Geophys Res*. <https://doi.org/10.1029/2005JD005850>
- Jain A et al (2010) Mesoscale convection system and occurrence of extreme low tropopause temperatures: observations over Asian summer monsoon region. In: Jain AR, Panwar V (eds) *Annales Geophysicae*. European Geosciences Union, Munich, pp 927–940
- Jain A et al (2011) Occurrence of extremely low cold point tropopause temperature during summer monsoon season: ARMEX campaign and CHAMP and COSMIC satellite observations. *J Geophys Res*. <https://doi.org/10.1029/2010JD014340>
- Jing P, Cunnold DM, Wang R, Yang E (2004) Isentropic cross-tropopause ozone transport in the northern hemisphere. *J Atmos Sci* 61(9):1068–1078. [https://doi.org/10.1175/1520-0469\(2004\)061%3c1068:ICOTIT%3e2.0.CO;2](https://doi.org/10.1175/1520-0469(2004)061%3c1068:ICOTIT%3e2.0.CO;2)
- Johnson RH, Kriete DC (1982) Thermodynamic and circulation characteristics, of winter monsoon tropical mesoscale convection. *Mon Weather Rev* 110:1898–1911
- Kim H, Dessler AE (2004) Observations of convective cooling in the tropical tropopause layer in AIRS data. *Atmos Chem Phys*. <https://doi.org/10.5194/acpd-4-7615-2004>
- Kim J, Son S-W (2012) Tropical cold-point tropopause: Climatology, seasonal cycle, and intraseasonal variability derived from COSMIC GPS radio occultation measurements. *J Clim* 25:5343–5360
- Kim J, Randel WJ, Birner T (2018) Convectively driven tropopause-level cooling and its influences on stratospheric moisture. *J Geophys Res* 123:590–606
- Kizu N et al. (2018) Technical characteristics and GRUAN data processing for the Meisei RS-11G and iMS-100 radiosondes, GRUAN Technical document: 5
- Kodera K (2006) Influence of stratospheric sudden warming on the equatorial troposphere. *Geophys Res Lett*. <https://doi.org/10.1029/2005GL024510>
- Kuang Z, Bretherton CS (2004) Convective influence on the heat balance of the tropical tropopause layer: a cloud-resolving model study. *J Atmos Sci* 61:2919–2927
- Kumar KK (2006) VHF radar observations of convectively generated gravity waves: Some new insights. *Geophys Res Lett*. <https://doi.org/10.1029/2005GL024109>
- Matsuno T (1966) Quasi-geostrophic motions in the equatorial area. *J Meteorol Soc Jpn Ser II* 44:25–43
- McIntyre ME, Palmer TN (1983) Breaking planetary waves in the stratosphere. *Nature* 305(5935):593–600. <https://doi.org/10.1038/305593a0>
- Meenu S, Rajeev K, Parameswaran K, Nair AKM (2010) Regional distribution of deep clouds and cloud top altitudes over the Indian subcontinent and the surrounding oceans. *J Geophys Res*. <https://doi.org/10.1029/2009JD011802>
- Mehta SK, Venkat Ratnam M, Krishna Murthy B (2010) Variability of the tropical tropopause over Indian monsoon region. *J Geophys Res*. <https://doi.org/10.1029/2009JD012655>

- Mehta SK, Ratnam MV, Krishna Murthy B (2011a) Multiple tropopauses in the tropics: a cold point approach. *J Geophys Res.* <https://doi.org/10.1029/2011JD016637>
- Mehta SK, Ratnam MV, Murthy BK (2011b) Characteristics of the tropical tropopause over different longitudes. *J Atmos Solar Terr Phys* 73:2462–2473
- Mehta SK, Ratnam MV, Murthy BK (2013) Characteristics of the multiple tropopauses in the tropics. *J Atmos Solar Terr Phys* 95:78–86
- Muhsin M et al (2018) Effect of convection on the thermal structure of the troposphere and lower stratosphere including the tropical tropopause layer in the South Asian monsoon region. *J Atmos Solar Terr Phys* 169:52–65
- Munchak LA, Pan LL (2014) Separation of the lapse rate and the cold point tropopauses in the tropics and the resulting impact on cloud top-tropopause relationships. *J Geophys Res* 119:7963–7978
- Nath D, Sridharan S, Sathishkumar S, Gurubaran S, Chen W (2013) Lower stratospheric gravity wave activity over Gadanki (13.5° N, 79.2° E) during the stratospheric sudden warming of 2009: Link with potential vorticity intrusion near Indian sector. *J Atmos Solar Terr Phys* 94(2013):54–64
- Newell RE, Gould-Stewart S (1981) A stratospheric fountain? *J Atmos Sci* 38:2789–2796
- Norton WA (1994) Breaking Rossby waves in a model stratosphere diagnosed by a vortex-following coordinate system and a technique for advecting material contours. *J Atmos Sci* 51(4):654–673. [https://doi.org/10.1175/1520-0469\(1994\)051%3c0654:BRWIAM%3e2.0.CO;2](https://doi.org/10.1175/1520-0469(1994)051%3c0654:BRWIAM%3e2.0.CO;2)
- Norton W (2006) Tropical wave driving of the annual cycle in tropical tropopause temperatures part II: model results. *J Atmos Sci* 63:1420–1431
- Pan L, Randel W, Gary B, Mahoney M, Hintsa E (2004) Definitions and sharpness of the extratropical tropopause: a trace gas perspective. *J Geophys Res.* <https://doi.org/10.1029/2004JD004982>
- Paulik LC, Birner T (2012) Quantifying the deep convective temperature signal within the tropical tropopause layer (TTL). *Atmos Chem Phys.* <https://doi.org/10.5194/acp-12-12183-2012>
- Pommereau J-P, Held G (2007) Is there a stratospheric fountain? *Atmos Chem Phys Discuss* 7:8933–8950
- Randel WJ, Wu F (2005) Kelvin wave variability near the equatorial tropopause observed in GPS radio occultation measurements. *J Geophys Res.* <https://doi.org/10.1029/2004JD005006>
- Randel WJ, Wu F, Gaffen DJ (2000) Interannual variability of the tropical tropopause derived from radiosonde data and NCEP reanalyses. *J Geophys Res* 105:15509–15523
- Randel WJ, Wu F, Rivera Ríos W (2003) Thermal variability of the tropical tropopause region derived from GPS/MET observations. *J Geophys Res.* <https://doi.org/10.1029/2002JD002595>
- Ratnam MV, Tsuda T, Shiotani M, Fujiwara M (2005) New characteristics of the tropical tropopause revealed by CHAMP/GPS measurements. *Sola* 1:185–188
- Ratnam MV, Tsuda T, Kozu T, Mori S (2006) Long-term behavior of the Kelvin waves revealed by CHAMP/GPS RO measurements and their effects on the tropopause structure. *Ann Geophys.* <https://doi.org/10.5194/angeo-24-1355-2006>
- Reid G, Gage K (1996) The tropical tropopause over the western Pacific: wave driving, convection, and the annual cycle. *J Geophys Res* 101:21233–21241
- Resmi E, Mohanakumar K, Appu K (2013) Effect of polar sudden stratospheric warming on the tropical stratosphere and troposphere and its surface signatures over the Indian region. *J Atmos Solar Terr Phys* 105:15–29
- Roy C, Fadnavis S, Sabin T (2021) The stratospheric ozone rich cold intrusion during El-Niño over the Indian region: Implication during the Indian summer monsoon. *Int J Climatol* 41:E233–E248
- Satheesan K, Murthy BK (2005) Modulation of tropical tropopause by wave disturbances. *J Atmos Solar Terr Phys* 67:878–883
- Schmidt T, Wickert J, Beyerle G, Reigber C (2004) Tropical tropopause parameters derived from GPS radio occultation measurements with CHAMP. *J Geophys Res.* <https://doi.org/10.1029/2004JD004566>
- Seidel DJ, Ross RJ, Angell JK, Reid GC (2001) Climatological characteristics of the tropical tropopause as revealed by radiosondes. *J Geophys Res* 106:7857–7878
- Selkirk HB (1993) The tropopause cold trap in the Australian monsoon during STEP/AMEX 1987. *J Geophys Res* 98:8591–8610
- Shepherd TG (2002) Issues in stratosphere-troposphere coupling. *J Meteorol Soc Jpn Ser II* 80:769–792
- Sherwood P et al (2003) QUASI: A general purpose implementation of the QM/MM approach and its application to problems in catalysis. *J Mol Struct (theochem)* 632:1–28
- Shi C, Cai W, Guo D (2017) Composition and thermal structure of the upper troposphere and lower stratosphere in a penetrating mesoscale convective complex determined by satellite observations and model simulations. *Adv Meteorol.* <https://doi.org/10.1155/2017/6404796>
- Son SW, Tandon NF, Polvani LM (2011) The fine-scale structure of the global tropopause derived from COSMIC GPS radio occultation measurements. *J Geophys Res.* <https://doi.org/10.1029/2011JD016030>
- Sunilkumar S, Babu A, Parameswaran K (2013) Mean structure of the tropical tropopause and its variability over the Indian longitude sector. *Clim Dyn* 40:1125–1140
- Takashima H, Eguchi N, Read W (2010) A short-duration cooling event around the tropical tropopause and its effect on water vapor. *Geophys Res Lett.* <https://doi.org/10.1029/2010GL044505>
- Tsuda T, Murayama Y, Wiryosumarto H, Harijono SWB, Kato S (1994) Radiosonde observations of equatorial atmosphere dynamics over Indonesia: 1. Equatorial waves and diurnal tides. *J Geophys Res* 99:10491–10505
- Venkat Ratnam M et al (2016) Effect of tropical cyclones on the stratosphere–troposphere exchange observed using satellite observations over the north Indian Ocean. *Atmos Chem Phys* 16:8581–8591
- Vömel H et al (2007) Radiation dry bias of the Vaisala RS92 humidity sensor. *J Atmos Ocean Tech* 24:953–963
- Wang JS, Seidel DJ, Free M (2012) How well do we know recent climate trends at the tropical tropopause? *J Geophys Res.* <https://doi.org/10.1029/2012JD017444>
- Waugh DW, Polvani LM (2000) Climatology of intrusions into the tropical upper troposphere. *Geophys Res Lett* 27:3857–3860
- Webster PJ, Stephens GL (1980) Tropical upper-tropospheric extended clouds: inferences from winter MONEX. *J Atmos Sci* 37:1521–1541
- Xian T, Fu Y (2015) Characteristics of tropopause-penetrating convection determined by TRMM and COSMIC GPS radio occultation measurements. *J Geophys Res* 120:7006–7024
- Yamamoto MK, Oyamatsu M, Horinouchi T, Hashiguchi H, Fukao S (2003) High time resolution determination of the tropical tropopause by the Equatorial Atmosphere Radar. *Geophys Res Lett.* <https://doi.org/10.1029/2003GL018072>
- Yoshida K, Yamazaki K (2011) Tropical cooling in the case of stratospheric sudden warming in, focus on the tropical tropopause layer. *Atmos Chem Phys* 11(2011):6325–6336

Publisher's Note Springer Nature remains neutral with regard to jurisdictional claims in published maps and institutional affiliations.